

Robust Causal Discovery in Real-World Time Series with Power-Laws

Matteo Tusoni *

Department of Computer Science,
Sapienza, University of Rome
Banca d'Italia ^{†‡}
matteo.tusoni@uniroma1.it

Giuseppe Masi

Department of Computer Science
Sapienza, University of Rome

Andrea Coletta

Banca d'Italia [†]

Aldo Glielmo

Banca d'Italia [†]

Viviana Arrigoni

Department of Computer Science
Sapienza, University of Rome

Novella Bartolini

Department of Computer Science
Sapienza, University of Rome

Abstract

Exploring causal relationships in stochastic time series is a challenging yet crucial task with a vast range of applications, including finance, economics, neuroscience, and climate science. Many algorithms for Causal Discovery (CD) have been proposed, but they often exhibit a high sensitivity to noise, resulting in misleading causal inferences when applied to real data. In this paper, we observe that the frequency spectra of typical real-world time series follow a power-law distribution, notably due to an inherent self-organizing behavior. Leveraging this insight, we build a robust CD method based on the extraction of power-law spectral features that amplify genuine causal signals. Our method consistently outperforms state-of-the-art alternatives on both synthetic benchmarks and real-world datasets with known causal structures, demonstrating its robustness and practical relevance.

1 Introduction

Causal Discovery (CD) from stochastic time series aims to identify causal relationships among time-evolving variables purely from observational data. CD algorithms represent a domain-agnostic alternative to analytical modeling, which can be impractical in many scientific domains characterized by complex dynamics. The resulting causal model is typically represented with a *causal graph*, where nodes are variables, and directed edges reflect asymmetric causal dependencies between them. This methodology has been successfully employed on a vast range of fields, including climate science [1, 2], neuroscience [3, 4], finance [5, 6], and, more recently, generative AI [7, 8, 9]. Nevertheless, inferring causal relationships in time series is particularly challenging due to factors such as noise and non-stationarity (i.e., time-varying dynamics) which can obscure the underlying causal structure and reducing the robustness of causal discovery algorithms.

Classical CD methods, most notably Granger Causality and its immediate extensions, rely on restrictive assumptions such as noise stationarity and the existence of a single characteristic scale

*Corresponding author

[†]This research was conducted as part of an internship at Banca d'Italia.

[‡]Views and opinions are those of the authors and do not necessarily reflect the official policy or position of Banca d'Italia.

to appropriately define vector-autoregressive (VAR) models. Unfortunately, these assumptions are frequently violated, as real-world systems are typically non-equilibrium, history-dependent, often displaying scale-free temporal correlations and power-law frequency spectra [10]. In such contexts, conventional CD algorithms can easily incur errors, and detect spurious relationships or fail to detect true interactions.

To address these shortcomings, we introduce **PLaCy** (Power-Law Causal discovery), which is specifically designed to leverage the scale-free properties commonly observed in real-world time series. Instead of comparing variables at individual time points, it fits a power-law model to the frequency spectrum of each process and tracks the evolution of the fitted spectral exponents and amplitudes. In this way, **PLaCy** isolates structural causal changes that propagate from one variable to another by filtering out non-stationary and nonlinear external influences, bearing the absence of a characteristic scale. Classical Granger-type hypothesis tests are then applied to the trajectories of power-law spectral exponents and amplitudes, rather than to the raw signals, preserving the statistical power of established testing theory.

By running extensive experiments on synthetic benchmarks with controlled nonlinear and non-stationary noise, or scale-free characteristics, as well as on two real-world data sets, we demonstrate that **PLaCy** outperforms state-of-the-art CD methods, particularly in regimes where the nonequilibrium, nonlinear, or scale-free properties of the time series are more pronounced.

The main contribution of this paper is the following:

- We propose **PLaCy**, a novel framework that leverages spectral trends for robust causal discovery in time-series with power-law frequency distributions.
- We theoretically demonstrate that the frequency-domain transformation used in **PLaCy** preserves the underlying causal graph structure, guaranteeing results consistent with the time-domain graph.
- We empirically show that **PLaCy** provides more robust and accurate estimations, validated through extensive experiments on both synthetic and real-world datasets.

2 Preliminaries

2.1 Background

Causal Relationship Let $\mathbf{x} = (\mathbf{x}_1, \mathbf{x}_2, \dots, \mathbf{x}_d)$ be a d -dimensional multivariate time series of length L . We say that a variable \mathbf{x}_i has a *causal effect* on another variable \mathbf{x}_j if a change in \mathbf{x}_i influences (or causes) the behavior or distribution of \mathbf{x}_j . Following Pearl’s definition [11], a variable \mathbf{x}_i is said to *cause* \mathbf{x}_j (denoted $\mathbf{x}_i \rightarrow \mathbf{x}_j$) if an intervention on \mathbf{x}_i , denoted $do(\mathbf{x}_i)$, changes the marginal distribution of \mathbf{x}_j , i.e.,

$$P(\mathbf{x}_j \mid do(\mathbf{x}_i)) \neq P(\mathbf{x}_j).$$

In most practical cases, active interventions on the system are unfeasible, and only observational data are available. While Pearl’s framework allows causal inference from observational data under specific assumptions (e.g., the backdoor criterion), these conditions are not always satisfied or verifiable. In such cases, Granger causality is widely adopted as a practical alternative to infer causal relationships.

Granger Causality The Granger’s causality definition is based on whether one time series provides statistically significant information to forecast another [12]. In particular, we say that \mathbf{x}_i *Granger-causes* \mathbf{x}_j if the past values of \mathbf{x}_i are useful to predict \mathbf{x}_j , given the past of all other time series. In time series data, Granger causality is typically studied using a multivariate vector autoregressive model (VAR) [13]:

$$\mathbf{x}(t) = \sum_{\tau=1}^T \mathbf{A}_{\tau} \mathbf{x}(t - \tau) + \boldsymbol{\varepsilon}_t,$$

where $\mathbf{x}(t)$ represents the multivariate time-series at time t , with each component defined as a linear combination of the past T values of all variables. Granger causal analysis involves fitting a VAR model and testing the statistical significance of the autoregressive coefficient matrices \mathbf{A}_{τ} , typically using a Wald test [14]. This requires comparing two models: the unrestricted model, which includes lagged terms of both \mathbf{x}_i and \mathbf{x}_j , and the restricted model, which excludes the lagged terms of \mathbf{x}_i from the prediction of \mathbf{x}_j . The null hypothesis states that all coefficients related to the lagged \mathbf{x}_i terms are zero. Failing to reject this null hypothesis implies that \mathbf{x}_i does not Granger-cause \mathbf{x}_j .

Notice that the Granger causality definition does not explicitly account for the time elapsed between cause and effect, since it jointly tests all specified lags together. Similarly, in our work, we focus on

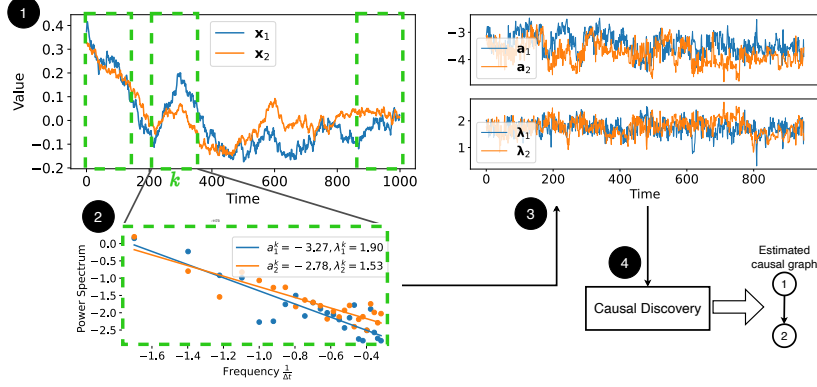


Figure 1: **Schematic illustration of the proposed methodology.** The original time series, here x_1 and x_2 , are first segmented into overlapping windows (**step 1**). Then, for each window k , the amplitudes (a_1^k, a_2^k) and the exponents (λ_1^k, λ_2^k) of the power-law distributed spectra are computed (**step 2**). These give rise to new, multi-dimensional, time series: (a_1, λ_1) for x_1 and (a_2, λ_2) for x_2 respectively (**step 3**). Finally, multivariate Granger causality tests are performed on these new series, and the causal graph is constructed (**step 4**).

identifying the existence of causal relationships, regardless of the specific time lag between cause and effect.

2.2 Task definition

Causal Discovery is the task of identifying the underlying structure of cause-and-effect relationships among the components of a multivariate system. Given a collection of observed multivariate time series, the goal is to infer a directed graph that encodes which variables influence others in a causal sense. Formally, given a time-series $\mathbf{x} \in \mathbb{R}^{L \times d}$, the task is to determine a directed graph $G = (V, E)$, where $V = \{1, 2, \dots, d\}$ represents the variables of the system, and $E \subseteq V \times V$ is the set of directed edges. A directed edge (i, j) exists if and only if x_i is inferred to be a cause of x_j . The goal of our approach is to derive the causal graph representing the causal relationships among the variables.

2.3 Power-laws in the real-world

An abundance of empirical evidence has accumulated over the past six decades showing that power-law spectra of the type $S(f) \propto f^{-\lambda}$, with $\lambda > 0$, are ubiquitous for real-world time series. Classic examples can be found in finance [15, 16], climate science [17, 18] or neuroscience [19, 20, 21, 22]. Power-law spectra frequently arise in systems composed of many interacting units, such as traders in a market or nodes in communication networks, that *self-organize* into structured behavior without any external regulator/coordinator [23, 24]. Specifically, self-organizing systems often exhibit scale invariance [25], precisely due to the absence of any external coordinator enforcing a characteristic scale. A stochastic process $\{x(t)\}$, is *scale invariant* if $\forall a \in \mathbb{R}^+$, the rescaled process $\{x(at)\}$ is statistically equivalent to $\{a^H x(t)\}$, for some $H \in \mathbb{R}^+$. In practice, the above-defined property implies that any magnified fragment of a scale-invariant stochastic process looks identical to the original series and, for this reason, scale invariance is sometimes referred to as self-similarity and is very related to the geometric concept of a fractal [10]. It is also known that, under very loose assumptions, scale-invariant stochastic processes are also *scale-free*, meaning that they exhibit power-law correlations, and power-law distributed frequency spectra with exponent $\lambda = 2H - 1$ [26]. Given the ubiquity of power-law distributed frequency spectra in the real-world, this structural regularity can be leveraged to improve the extraction of causal signals from time series, reducing spurious temporal dependencies.

3 Proposed Methodology

A well-established approach in signal processing involves analyzing the frequency content of a signal via its spectral representation. To this end, we employ the Discrete Fourier Transform (DFT). Given a real-valued time series $x(t)$ of length L , the DFT is defined as:

$$\phi(k) = \sum_{t=0}^{L-1} x(t) e^{-i2\pi \frac{k}{L} t}, \quad k \in \{0, \dots, L-1\}, \quad (1)$$

where $\phi(k) \in \mathbb{C}$ denotes the complex-valued coefficient corresponding to the k -th discrete frequency. The associated normalized frequency is given by $f_k = \frac{k}{L}$. The magnitude of each Fourier coefficient quantifies the contribution of the corresponding frequency component to the overall signal. We therefore define the *spectral amplitude* as: $A(f_k) = |\phi(k)|$.

As discussed previously, many natural and social systems exhibit long-range dependencies and scale-free behavior in their frequency content, often associated with self-organized phenomena. A defining characteristic of these systems is the power-law decay of their power spectral amplitude, typically modeled as: $A(f) = e^a \cdot f^{-\lambda}$, where e^a is a scaling constant and $\lambda > 0$ is the *spectral exponent*. The exponent λ is tightly linked to structural features of the process, such as its autocorrelation. Importantly, the spectral parameters a and λ may vary over time due to exogenous perturbations or endogenous interactions. These variations provide an opportunity to study causal structures through their temporal dynamics. Instead of analyzing the raw time series directly, we propose to monitor the evolution of (a, λ) as informative summaries of the underlying processes. To achieve this, we segment each time series into overlapping windows (**step 1** in Figure 1) and compute the local spectral parameters within each window. This is done by estimating the slope and intercept of the spectrum in log-log space:

$$\log A(f) = a - \lambda \log f. \quad (2)$$

The linear form permits efficient estimation via ordinary least squares, yielding one value of a and λ per window (**step 2** in Figure 1). Repeating this procedure across the entire series results in two new time series per original signal: \mathbf{a} and $\boldsymbol{\lambda}$ (**step 3** in Figure 1).

To capture the spectral behavior exhibited within each analysis window, we apply overlapping windows. This design is critical to preserve the detection of short-lived or temporally localized causal effects. To maximize sensitivity, the stride between consecutive windows is fixed at 1, so that each new window shifts by a single time step. This dense sampling guarantees that even subtle or rapid changes in the spectral parameters (a, λ) are preserved in the constructed feature time series. The window length is selected adaptively to balance two competing requirements: it must be short enough to capture temporal variations in the spectral parameters, yet long enough to ensure a reliable estimation of the power-law behavior. To meet this trade-off, we evaluate the p -value of a Wald test on the linear fit in log-log space for each candidate window size, and select the shortest window for which the fit achieves a statistical significance threshold of $p = 0.05$. Further details of this procedure are provided in the Appendix.

Once the feature series $(\mathbf{a}, \boldsymbol{\lambda})$ are built for a couple of original signals, we perform multivariate Granger causality tests, as described in Section 2.1 (**step 4** in Figure 1). Since the causal information is primarily encoded in the λ parameter, the Granger test is applied to assess whether $(\lambda_i, \mathbf{a}_i)$ of the candidate causing series \mathbf{x}_i provide statistically significant information about the dynamics of λ_j in the target series \mathbf{x}_j (see Appendix). In the end, a causal edge is retained in the resulting graph if the corresponding p -value falls below the fixed threshold of 0.05. This procedure is repeated across all variable pairs to reconstruct the full causal graph.

Algorithm 1: PLACY

Input: Time series $\mathbf{x} = (\mathbf{x}_1, \dots, \mathbf{x}_d)$ of length L ; stride s ; window size l .

Output: Causal Graph \mathcal{G} .

- 1 Divide each \mathbf{x}_i into $\lfloor \frac{L-l}{s} \rfloor + 1$ sliding windows each, namely \mathbf{w}_i^k , of size l with stride s .
 - 2 **for** each $i \in \{1, \dots, d\}$ **do**
 - 3 **for** each $k \in \{0, \dots, \lfloor \frac{L-l}{s} \rfloor\}$ **do**
 - 4 Apply the DFT (Equation (1)) to \mathbf{w}_i^k to get ϕ_i^k .
 - 5 Obtain (a_i^k, λ_i^k) by using the fit in Equation (2) on ϕ_i^k .
 - 6 Concatenate the values (a_i^k, λ_i^k) over each k to obtain time series $(\mathbf{a}_i, \boldsymbol{\lambda}_i)$.
 - 7 **for** each $i, j \in \{1, \dots, d\}$ such that $i \neq j$ **do**
 - 8 $\mathcal{G}_{i,j} \leftarrow$ Granger Causality test 2.1 with $(\mathbf{a}_i, \boldsymbol{\lambda}_i)$ as causing series and $\boldsymbol{\lambda}_j$ as caused series.
 - 9 **return** \mathcal{G} .
-

3.1 Invariance of the Causal Graph under Spectral Feature Mapping

Unlike conventional Granger methods, which analyze lagged relationships in the original signal space, our approach infers causality from the coordinated evolution of spectral properties. Moreover,

the spectral fitting acts as a natural denoising step, improving robustness to non-Gaussian fluctuations and high-frequency noise. In the following Theorem 1, we discuss the correctness of this approach by showing that the causal graph of a stochastic process is invariant under the spectral transformation applied in Algorithm 1, which preserves the causal semantics of the original process.

Theorem 1 (Invariance of the Causal Graph under Spectral Transformations). *Let \mathbf{x} be a multivariate time series generated by a structural causal process with associated ground-truth causal graph \mathcal{G}^* . Let \mathcal{T} be the spectral transformation described in Algorithm 1, which extracts from \mathbf{x}_i a set of time-evolving features $(\mathbf{a}_i, \boldsymbol{\lambda}_i)$. Then, under standard conditions for identifiability in vector autoregressive (VAR) models, the causal graph \mathcal{G}^* is structurally invariant under \mathcal{T} . That is, the causal dependencies encoded in \mathcal{G}^* remain valid when causal discovery is performed on the feature sequence $(\mathbf{a}, \boldsymbol{\lambda})$.*

Proof sketch. The proof proceeds in two steps. First, we show that the feature series $(\mathbf{a}, \boldsymbol{\lambda})$ satisfies the classical assumptions required for valid inference in vector autoregressive (VAR) models, as established in [13]. Second, we demonstrate that the mapping \mathcal{T} preserves the structure of the ground-truth causal graph \mathcal{G}^* , meaning that no spurious or missing edges are introduced by the transformation. Combining these two results, we conclude that applying Granger causality analysis to the transformed sequence $(\mathbf{a}, \boldsymbol{\lambda})$ successfully recovers the true underlying causal graph \mathcal{G}^* . The complete formal proof of the Theorem 1 is provided in the Appendix. \square

4 Related Work

Causal discovery from observational time series has been extensively studied [27, 28], leading to a broad spectrum of methods, from classical statistical tests to more advanced machine learning and spectral approaches. We review many of them here, highlighting in **bold** the ones we compare against in this work. Moving beyond **Granger Causality** described in Section 2.1, constraint-based methods have been developed and adapted for the temporal domain. Notably, the PC (Peter–Clark) algorithm [29] (and its extension, FCI [30]) serves as the foundation for several approaches. These utilize conditional independence tests to infer graphical causal structures while accounting for temporal ordering. Building on these, the **PCMCI** algorithm [31] enhances causal discovery in time series by combining the PC methodology with the Momentary Conditional Independence (MCI) test, which rigorously controls for autocorrelation and indirect associations. This algorithm was recently extended with **PCMCI $_{\Omega}$** [32] to the case of semi-stationary structural causal models. Optimization-based and deep-learning approaches have further broadened the field. **DYNOTEARS** [33] casts causal discovery as a continuous optimization problem subject to acyclicity constraints, preserving efficiency in handling high-dimensional data. **Rhino** [34] represents an innovative deep learning-based approach where the CD task is addressed in scenarios where the noise distributions may depend on historical information. On the one hand, the use of neural networks allows Rhino to handle history-dependent and non-stationary noise; on the other hand, this advantage comes at the cost of significant computational overhead during training. Other techniques, such as Convergent Cross Mapping (CCM) [35], although robust in theory, exhibit significant performance degradation in noisy settings. Recent efforts have been made to enhance the noise-resilience of existing algorithms. **CCM-Filtering** [36] improves the performance of CCM by simply pre-processing the time series with an averaging filter. **RCV-VarLiNGAM** [37] integrates the K -fold cross-validation technique with the VarLiNGAM method [38], addressing the challenges of a lack of noise robustness encountered in the standard method.

Previous works have also studied frequency-domain causal discovery. **Geweke**’s seminal work [39] extended Granger causality by assessing causal interactions at specific frequencies, offering insights into dynamic interdependencies often hidden in time-domain analyses. Subsequent works applied this method in domain-specific scenarios, such as economic cycles and oscillatory phenomena [40], network and finance [41], commodity markets [42], and market volatility [43].

Despite these advancements, current frequency-domain methods remain vulnerable to noise, spurious dependencies, and deviations from Gaussianity. Motivated by these limitations, our method builds upon the spectral causality definition introduced by Geweke and proposes an advanced spectral trend modeling to effectively separate meaningful causal signals from noise-induced artefacts. Our approach inherently leverages the frequency-dependent structure of power-law processes, enhancing resilience to nonlinear complex noisy signals.

In the next section, the conducted experiments demonstrate that our algorithm outperforms the most competitive cited methods (highlighted in bold) in a broad range of scenarios while maintaining sample-level inference efficiency.

5 Experiments

Unless otherwise stated, our method employs a sliding window of size $l = 50$, selected through the p -value procedure outlined in Section 3, and a stride $s = 1$ (refer to Algorithm 1). Quantitative results are averaged over 100 runs for all methods, except for Rhino, which is averaged over only 10 random seeds due to the high computational cost of neural network training. The code for all experiments is publicly available⁴.

We consider both synthetic and real-world datasets to rigorously evaluate the main claims of our approach, namely, its robustness to noise and spurious associations in real-world time series whose frequency spectra follow a power-law distribution. In particular, we create four synthetic datasets with increasing complexity, and we consider two real-world benchmark datasets with known causal graphs. Some prior datasets were excluded due to the absence of ground-truth causal graph or insufficient time series length for spectral estimation.

Metrics We evaluate the performance of the algorithms based on their ability to accurately identify causal relationships among variables. By comparing the edges of the predicted causal graph with those of the ground-truth graph, we compute the following metrics: *F1-score* (F1) that measures the performance of algorithms in correctly identifying causal relationships; and *True Negative Rate* (TNR) to evaluate the robustness of the algorithms to noise and spurious associations, by measuring its ability to correctly identify the absence of causal links. The latter metric is particularly insightful, as it evaluates a method’s ability to exclude erroneous relationships in the generated causal graphs, an aspect not directly captured by the F1-score.

5.1 Synthetic Scenarios

Data Generation To generate complex benchmark datasets, we use the well-known Ornstein-Uhlenbeck (OU) processes, originally introduced in statistical physics to describe the velocity of a Brownian particle under friction [44]. These stochastic processes are widely used to model systems exhibiting mean-reverting behavior and power-law spectral characteristics. For example, they have been applied to capture the complexity of financial data [45]. In the frequency domain, OU processes exhibit a characteristic power-law decay, reflecting the behavior of various natural systems that our approach seeks to address. We simulate the baseline dynamics of each time series using a generalized OU process, defined as follows:

$$x(t + \Delta t) = x(t) + \frac{\Delta t}{\tau_c} (\mu - x(t)) + (\sigma_b \epsilon_b(t) + \sigma_g^a \epsilon_g^a(t) + \sigma_g^m \epsilon_g^m(t) \cdot x(t)) \sqrt{\Delta t}, \quad (3)$$

where $\Delta t = 0.01$ is the time step, $\tau_c = 0.5$ denotes the timescale of mean reversion, and $\mu = 1$ is the long-term mean. $\forall t$, $\epsilon_b(t)$, $\epsilon_g^a(t)$, and $\epsilon_g^m(t)$ represent the noise terms modeled as independent stochastic variables: the first is Brownian noise, while the latter two are standard Gaussian white noise processes. Specifically, $\epsilon_g^a(t)$ is an additive noise component, whereas $\epsilon_g^m(t)$ acts as a multiplicative noise term that induces non-stationarity as its impact scales with the process value. The parameters σ_b , σ_g^a , and σ_g^m represent different sources of noise volatility. This formulation enables the system to capture both additive and multiplicative stochastic effects, which are common in real-world dynamic systems.

To represent causal relationships between different time series, we construct a Directed Acyclic Graph (DAG) \mathcal{G} , represented by an upper triangular adjacency matrix ($M \in \{0, 1\}^{N \times N}$), which enforces a unidirectional flow of causality and prevents cycles. Each entry in the matrix is randomly set to 1 with a probability of 0.3, indicating a causal influence from one series to another.

Finally, causal dependencies are introduced by applying the generated ground truth causal matrix to the time series. In particular, if $M_{i,j} = 1$, indicating that series i influences series j , then

$$\forall t, x_j(t) \leftarrow x_j(t) + C \cdot x_i(t - \tau),$$

⁴<https://github.com/matteotusoni/PLACy>

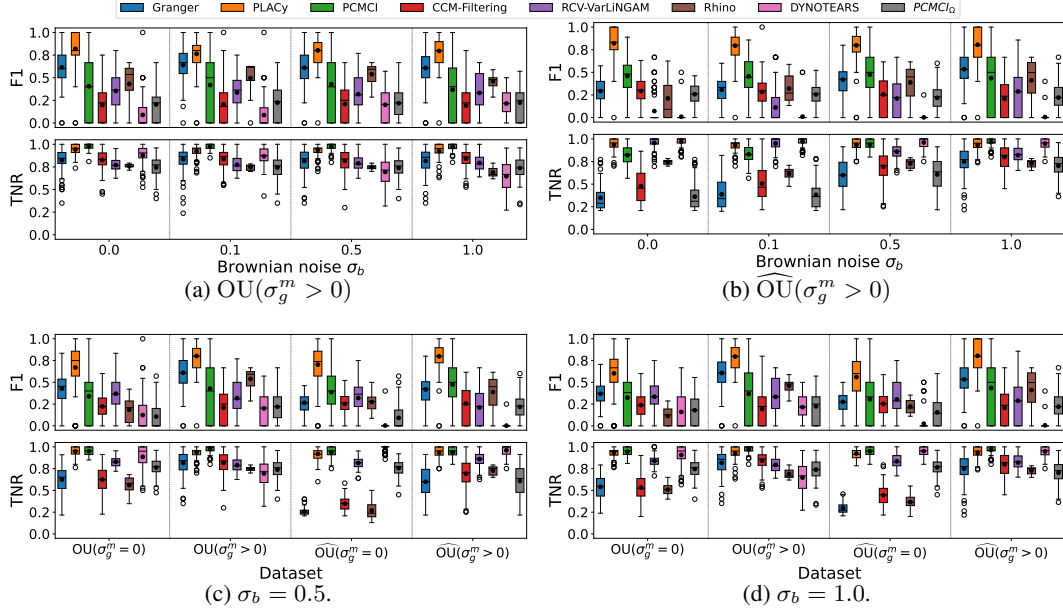


Figure 2: Results on synthetic datasets, with $N = 5$, $C = 0.5$, $\sigma_g^a = 1.0$.

where C represents the *causal strength*, and $\tau = 5$ is the number of time-steps between the cause and the effect. This ensures that the current value of the influenced series incorporates a lagged contribution from the influencing series. Finally, we scale all time series to their original range to remove any unintended amplifications or distortions during the causal injection.

Datasets Following the generation process described in the previous paragraph, we define four representative scenarios to evaluate the robustness of our method under different dynamic conditions according to Equation (3): **(1)** $\text{OU}(\sigma_g^m = 0)$ represents an OU process with no noise component proportional to the process itself; **(2)** $\text{OU}(\sigma_g^m > 0)$ includes a Gaussian noise term that is proportional to the current value of the process. Both processes are initialized in equilibrium conditions, with the first time step $t = 0$ set to 1.

Non-equilibrium and phase-transitioning systems display complex behaviors, as observed in several domains (e.g., in financial markets [46]). Therefore, we introduce a transition phase by initializing the process at 100. By extending the previous two scenarios, we obtain **(3)** $\widehat{\text{OU}}(\sigma_g^m = 0)$ and **(4)** $\widehat{\text{OU}}(\sigma_g^m > 0)$.

For each dataset, we generate different scenarios with $N = 5$ and $N = 10$ variables (i.e., time series), each of length $L = 5000$ time-steps.

Results Figure 2 reports the F1-score and the TNR obtained on synthetic datasets with $N = 5$ variables, causal strength $C = 0.5$ and $\sigma_g^a = 0$. A complete overview of the results can be found in Table 1 for the case of $N = 5$ and $\sigma_g^a = 1$, averaging over $\sigma_b \in \{0, 0.1, 0.5, 1\}$. Additional results, including scenarios with $N = 10$ and $\sigma_g^a = 0.5$, can be found in the Appendix.

Results for **Geweke** have been excluded from the plots of Figure 2 and Tables 1 and 2 due to its consistently poor performance. In particular, the *True Negative Rate* (TNR) across the same experimental settings is uniformly zero, as the method fails to reject any spurious connections.

Key takeaway: Our method consistently outperforms baseline approaches across all scenarios, demonstrating strong robustness to both structural variations and noise. In particular, Figures 2a and 2b show that our approach, **PLaCy**, achieves overall the best performance in terms of F1-score for all the noise settings σ_b , for $\text{OU}(\sigma_g^m > 0)$ and $\widehat{\text{OU}}(\sigma_g^m > 0)$. In fact, the presence of multiplicative Gaussian noise introduces non-stationarity, which is not correctly dealt with by conventional methods. **PLaCy** instead, by analyzing causal dynamics through spectral parameters, is able to effectively filter out the variability induced by the multiplicative noise in a way that traditional VAR-based approaches

Table 1: F1 Score - $N = 5$, $\sigma_g^a = 1.0$

	C	Granger	PLaCy	PCMCI	CCM-Filtering	RCV-VarLiNGAM	Rhino	DYNOTEARS	PCMCI $_{\Omega}$
$OU(\sigma_g^m = 0)$	0.2	0.58 ± 0.26	0.14 ± 0.22	0.15 ± 0.24	0.18 ± 0.18	0.40 ± 0.19	0.17 ± 0.12	0.17 ± 0.18	0.07 ± 0.13
	0.5	0.56 ± 0.25	0.73 ± 0.24	0.20 ± 0.27	0.19 ± 0.17	0.39 ± 0.19	0.19 ± 0.16	0.08 ± 0.18	0.11 ± 0.14
	1.0	0.53 ± 0.25	0.77 ± 0.17	0.28 ± 0.29	0.25 ± 0.19	0.32 ± 0.21	0.27 ± 0.14	0.08 ± 0.17	0.13 ± 0.15
$\widehat{OU}(\sigma_g^m = 0)$	0.2	0.47 ± 0.28	0.24 ± 0.25	0.16 ± 0.25	0.26 ± 0.12	0.41 ± 0.19	0.19 ± 0.13	0.02 ± 0.10	0.08 ± 0.13
	0.5	0.45 ± 0.27	0.69 ± 0.22	0.21 ± 0.26	0.26 ± 0.12	0.37 ± 0.20	0.22 ± 0.13	0.01 ± 0.06	0.10 ± 0.14
	1.0	0.45 ± 0.26	0.70 ± 0.17	0.29 ± 0.30	0.26 ± 0.11	0.32 ± 0.19	0.27 ± 0.12	0.01 ± 0.06	0.13 ± 0.15
$OU(\sigma_g^m > 0)$	0.2	0.63 ± 0.21	0.72 ± 0.24	0.23 ± 0.29	0.19 ± 0.21	0.39 ± 0.18	0.36 ± 0.19	0.22 ± 0.14	0.16 ± 0.16
	0.5	0.62 ± 0.20	0.80 ± 0.17	0.40 ± 0.33	0.20 ± 0.20	0.34 ± 0.20	0.48 ± 0.18	0.15 ± 0.17	0.22 ± 0.16
	1.0	0.57 ± 0.18	0.77 ± 0.18	0.60 ± 0.30	0.26 ± 0.21	0.28 ± 0.21	0.50 ± 0.12	0.17 ± 0.18	0.23 ± 0.18
$\widehat{OU}(\sigma_g^m > 0)$	0.2	0.39 ± 0.20	0.75 ± 0.21	0.32 ± 0.27	0.25 ± 0.17	0.22 ± 0.23	0.18 ± 0.19	0.02 ± 0.10	0.22 ± 0.14
	0.5	0.39 ± 0.18	0.80 ± 0.17	0.46 ± 0.26	0.26 ± 0.17	0.17 ± 0.21	0.33 ± 0.22	0.01 ± 0.05	0.24 ± 0.14
	1.0	0.39 ± 0.18	0.78 ± 0.17	0.55 ± 0.25	0.30 ± 0.16	0.15 ± 0.20	0.43 ± 0.17	0.01 ± 0.07	0.26 ± 0.14

cannot handle. When such multiplicative noise is not present, as shown in Figures 2c and 2d, **PLaCy** achieves the best performance also in all remaining synthetic scenarios, for fixed values of $\sigma_b = 0.5$ and $\sigma_b = 1$, respectively.

In all the experiments in Figure 2, the TNR of **PLaCy** is always very high, sometimes moderately outperformed by **PCMCI**. This is due to the fact that **PCMCI** is designed to explicitly control false positives, with a conservative approach to edge selection (MCI phase). **PLaCy**, however, shows a more permissive behavior in edge inclusion. This causes occasional acceptance of marginal causal association, but it is also the key to capturing genuine causal relations, as confirmed by the higher F1-score. Figure 2b considers the impact of both multiplicative noise and non-equilibrium initialization, two aspects that constitute a significant challenge for traditional CD approaches. In this setting, **PLaCy** significantly outperforms the other methods, with the highest F1-score and TNR close to 1, thanks to its capability to distinguish meaningful causal perturbations in spectral trends from spurious correlations possibly due to transient non-stationary dynamics. In the absence of multiplicative Gaussian noise, Figure 2d shows that standard causal inference methods that hardly rely on stationarity assumptions tend to struggle. Also in this scenario, **PLaCy** demonstrates robustness by capturing structural shifts in spectral parameters, identifying genuine causal relationships without confusing transient behaviors for structural causal patterns.

The inadequacy of **PCMCI** to deal with non-Gaussian and non-stationary noise is evident from the poor performance shown in the F1-score. The same limitations apply to its generalized version of this algorithm, i.e., **PCMCI $_{\Omega}$** (designed to handle semi-stationary causal relationships).

Regarding the other methods, although **Granger Causality** is not built to work with non-stationary and non-Gaussian noise, it retains a reasonable ability to understand causal relationships in such complex scenarios. Even if **CCM-Filtering** is designed to improve the robustness of the original CCM by reducing high-frequency noise and preserving lower-frequency signals, this solution does not generalize to stochastic processes, where delay embeddings fail to capture a deterministic manifold. **RCV-VarLiNGAM** does not show good results in a non-stationary noise environment, as expected by its assumption of stationarity. Although designed to uncover causal relationships via exploitation of non-Gaussian noise, the improvement with respect to other models remains limited. **DYNOTEARS** is designed to handle additive noise, but in our experiments, it struggles under multiplicative perturbations and strong non-stationarity. As a result, the method tends to miss true causal links, despite maintaining a high TNR. Finally, **Rhino** achieves reasonable performances as proved by the experiments in Figures 2a and 2b, validating the authors' claim that the method is

Table 2: Performance comparison on real-world datasets.

		Granger	PLaCy	PCMCI	CCM-Filtering	RCV-VarLiNGAM	Rhino	DYNOTEARS	PCMCI Ω
Rivers	F1	0.47 \pm 0.07	0.51 \pm 0.10	0.47 \pm 0.07	0.28 \pm 0.01	0.16 \pm 0.12	0.29 \pm 0.03	0.12 \pm 0.07	0.10 \pm 0.09
	TNR	0.64 \pm 0.09	0.75 \pm 0.13	0.74 \pm 0.05	0.19 \pm 0.00	0.51 \pm 0.12	0.35 \pm 0.05	0.53 \pm 0.06	0.57 \pm 0.05
AirQuality	F1	0.41 \pm 0.02	0.45 \pm 0.04	0.25 \pm 0.03	0.40 \pm 0.00	—	0.44 \pm 0.01	0.37 \pm 0.08	0.36 \pm 0.04
	TNR	0.22 \pm 0.05	0.66 \pm 0.07	0.95 \pm 0.02	0.04 \pm 0.00	—	0.23 \pm 0.04	0.92 \pm 0.03	0.69 \pm 0.07

robust to increasing non-Gaussian noise. However, its computational complexity does not justify the lower performance compared to our approach, which also preserves sample efficiency.

5.2 Real Data Scenarios

As real-world scenarios, we consider two datasets with known causal graphs:

- **Rivers** dataset⁵ [47] contains $N = 6$ time series from three hydrological stations located in southern Germany, namely Dillingen, Kempten, and Lenggries. For each location, both river flow (or level) and local precipitation are measured across several thousand time steps. Since the Iller feeds into the Danube, increases in its discharge are expected to impact the Danube with a one-day lag.
- **AirQuality** dataset⁶ [48] contains hourly PM2.5 pollution measurements collected over one year from $N = 36$ monitoring stations across various Chinese cities. The ground-truth causal graph is derived from a causal matrix based on pairwise sensor distances.

In this case, several samples are extracted from the original time series with a length $L = 500$.

Results Table 2 reports the results for both datasets. Our method achieves overall competitive or the best performance in terms of F1-score and TNR for both datasets.

Key takeaway: The Rivers dataset poses an additional challenge due to its heterogeneous dynamics and the presence of exogenous factors such as seasonal precipitation. Because precipitation series lack clear power-law behavior, this dataset highlights PLaCy’s ability to generalize beyond its core assumptions.

Indeed, our method achieves robust performance and surpasses the other methods in detecting the causal effects of precipitation and rivers’ flow in both F1 and TNR.

On the other hand, the AirQuality dataset includes missing values, which were filled using linear interpolation. Missing data, common in environmental datasets, challenges most CD methods. **PLaCy** maintains competitive performance despite these imperfections, highlighting its robustness to real-world data issues thanks to the advantages of performing causal discovery in the frequency domain, which is inherently more resilient to missing data and noise. **RCV-VarLiNGAM**, failed to converge. In our tests, we observe that this behavior is due to the impossibility of running the Cholesky decomposition on the residual covariance matrix, which results in being non-positive definite as a consequence of missing data.

Despite the original CCM promises to be robust in correctly excluding causal links between non-coupled variables in the presence of external forcing, the performance of **CCM-Filtering**, and in particular the achieved TNR, degrades on more complex data, influenced by unobserved exogenous factors. The same considerations mentioned about the TNR attained by **PCMCI** on the synthetic datasets hold on AirQuality, where the high TNR is achieved at the expense of the lowest F1.

⁵Bavarian Environmental Agency data provider: <https://www.gkd.bayern.de>.

⁶Microsoft data provider: <https://www.microsoft.com/en-us/research/project/urban-computing>.

6 Limitations

Despite the strong performance demonstrated in the experimental campaign described in Section 5, **PLaCy** presents some limitations that should be acknowledged. First, it is not able to assess causal relationships in the presence of slowly varying spectra. Some strategies may improve the algorithm’s performance in such scenarios, such as increasing the number of lags considered in the causal analysis or extending the length of the analysis window (see Appendix). Nevertheless, in these cases, time-domain analyses like Granger causality may be more appropriate. While this represents a limitation, a reasonable choice of the causal analysis method can be guided by a preliminary spectral inspection. Second, the method is not well suited for very short time series, as it relies on local spectral estimation, which requires a minimum sequence length to produce stable features.

7 Conclusions

This study introduces **PLaCy**, a novel algorithm for causal discovery in stochastic time series, leveraging power spectrum analysis to identify underlying causal structures. An extensive experimental campaign on both synthetic and real-world datasets reveals the effectiveness of this methodology in comparison to state-of-the-art methods. Our findings underscore the advantages of frequency-domain analysis for causal discovery, highlighting its potential to avoid detecting spurious associations as causal relationships while maintaining high F1 scores. Future work will focus on extending the idea of exploiting the power spectrum to enhance non-VAR causal discovery methods. A deeper investigation should be conducted on the summary statistical parameters of the spectral density. Furthermore, an additional study must be conducted to address the possible presence of latent confounders.

References

- [1] Timothy J Mosedale, David B Stephenson, Matthew Collins, and Terence C Mills. Granger causality of coupled climate processes: Ocean feedback on the north atlantic oscillation. *Journal of climate*, 19(7):1182–1194, 2006.
- [2] Peer Nowack, Jakob Runge, Veronika Eyring, and Joanna D Haigh. Causal networks for climate model evaluation and constrained projections. *Nature communications*, 11(1):1415, 2020.
- [3] Steven L Bressler and Anil K Seth. Wiener–granger causality: a well established methodology. *Neuroimage*, 58(2):323–329, 2011.
- [4] Anil K Seth, Adam B Barrett, and Lionel Barnett. Granger causality analysis in neuroscience and neuroimaging. *Journal of Neuroscience*, 35(8):3293–3297, 2015.
- [5] Monica Billio, Mila Getmansky, Andrew W Lo, and Loriana Pelizzon. Econometric measures of connectedness and systemic risk in the finance and insurance sectors. *Journal of financial economics*, 104(3):535–559, 2012.
- [6] Francis X Diebold and Kamil Yılmaz. On the network topology of variance decompositions: Measuring the connectedness of financial firms. *Journal of econometrics*, 182(1):119–134, 2014.
- [7] Murat Kocaoglu, Christopher Snyder, Alexandros G Dimakis, and Sriram Vishwanath. Causalgan: Learning causal implicit generative models with adversarial training. *arXiv preprint arXiv:1709.02023*, 2017.
- [8] Mengyue Yang, Furui Liu, Zhitang Chen, Xinwei Shen, Jianye Hao, and Jun Wang. Causalvae: Disentangled representation learning via neural structural causal models. In *Proceedings of the IEEE/CVF conference on computer vision and pattern recognition*, pages 9593–9602, 2021.
- [9] Licheng Jiao, Yuhang Wang, Xu Liu, Lingling Li, Fang Liu, Wenping Ma, Yuwei Guo, Puhua Chen, Shuyuan Yang, and Biao Hou. Causal inference meets deep learning: A comprehensive survey. *Research*, 7:0467, 2024.
- [10] Per Bak. *How nature works: the science of self-organized criticality*. Springer Science & Business Media, 2013.
- [11] Judea Pearl. The do-calculus revisited. In *Proceedings of the Twenty-Eighth Conference on Uncertainty in Artificial Intelligence*, pages 3–11, 2012.
- [12] Clive W. J. Granger. Investigating causal relations by econometric models and cross-spectral methods. *Econometrica*, 37(3):424–438, 1969.
- [13] Helmut Lütkepohl. *New Introduction to Multiple Time Series Analysis*. Springer-Verlag, Berlin, Heidelberg, 2005.
- [14] Ludwig Fahrmeir, Thomas Kneib, Stefan Lang, and Brian D Marx. *Regression: Models, Methods and Applications*. Springer, 2013.
- [15] Giovanni Bonanno, Fabrizio Lillo, and Rosario N Mantegna. Dynamics of the number of trades of financial securities. *Physica A: Statistical Mechanics and its Applications*, 280(1-2):136–141, 2000.
- [16] Tiziana Di Matteo, Tomaso Aste, and Michel M Dacorogna. Long-term memories of developed and emerging markets: Using the scaling analysis to characterize their stage of development. *Journal of banking & finance*, 29(4):827–851, 2005.
- [17] Peter Huybers and William Curry. Links between annual, milankovitch and continuum temperature variability. *Nature*, 441(7091):329–332, 2006.
- [18] Hege-Beate Fredriksen and Kristoffer Rypdal. Spectral characteristics of instrumental and climate model surface temperatures. *Journal of Climate*, 29(4):1253–1268, 2016.
- [19] J. Matias Palva, Alexander Zhigalov, Jonni Hirvonen, Onerva Korhonen, Klaus Linkenkaer-Hansen, and Satu Palva. Neuronal long-range temporal correlations and avalanche dynamics are correlated with behavioral scaling laws. *Proceedings of the National Academy of Sciences*, 110(9):3585–3590, 2013.
- [20] Biyu J He. Scale-free brain activity: past, present, and future. *Trends in cognitive sciences*, 18(9):480–487, 2014.

- [21] Máté Gyurkovics, Grace M Clements, Kathy A Low, Monica Fabiani, and Gabriele Gratton. Stimulus-induced changes in 1/f-like background activity in eeg. *Journal of Neuroscience*, 42(37):7144–7151, 2022.
- [22] Vicente Medel, Martín Irani, Nicolás Crossley, Tomás Ossandón, and Gonzalo Boncompte. Complexity and 1/f slope jointly reflect brain states. *Scientific reports*, 13(1):21700, 2023.
- [23] Per Bak, Chao Tang, and Kurt Wiesenfeld. Self-organized criticality: An explanation of the 1/f noise. *Physical review letters*, 59(4):381, 1987.
- [24] Per Bak and Kan Chen. Self-organized criticality. *Scientific American*, 264(1):46–53, 1991.
- [25] Alex Proekt, Jayanth R Banavar, Amos Maritan, and Donald W Pfaff. Scale invariance in the dynamics of spontaneous behavior. *Proceedings of the National Academy of Sciences*, 109(26):10564–10569, 2012.
- [26] Patrick Flandrin. On the spectrum of fractional brownian motions. *IEEE Transactions on information theory*, 35(1):197–199, 1989.
- [27] C Gong, D Yao, C Zhang, W Li, and J Bi. Causal discovery from temporal data: An overview and new perspectives. *ACM Computing Surveys*, 2024.
- [28] Charles K Assaad, Emilie Devijver, and Eric Gaussier. Survey and evaluation of causal discovery methods for time series. *Journal of Artificial Intelligence Research*, 73:767–819, 2022.
- [29] Peter Spirtes, Clark N Glymour, and Richard Scheines. *Causation, prediction, and search*. MIT press, 2000.
- [30] Eric V Strobl, Shyam Visweswaran, and Peter L Spirtes. Fast causal inference with non-random missingness by test-wise deletion. *International journal of data science and analytics*, 6:47–62, 2018.
- [31] Jakob Runge, Peer Nowack, Marlene Kretschmer, Seth Flaxman, and Dino Sejdinovic. Detecting and quantifying causal associations in large nonlinear time series datasets. *Science advances*, 5(11):4996, 2019.
- [32] Shanyun Gao, Raghavendra Addanki, Tong Yu, Ryan Rossi, and Murat Kocaoglu. Causal discovery in semi-stationary time series. *Advances in Neural Information Processing Systems*, 36:46624–46657, 2023.
- [33] Roxana Pamfil, Nisara Sriwattanaworachai, Shaan Desai, Philip Pilgerstorfer, Konstantinos Georgatzis, Paul Beaumont, and Bryon Aragam. Dynotears: Structure learning from time-series data. In *International Conference on Artificial Intelligence and Statistics*, pages 1595–1605, 2020.
- [34] Wenbo Gong, Joel Jennings, Cheng Zhang, and Nick Pawlowski. Rhino: Deep causal temporal relationship learning with history-dependent noise. In *The Eleventh International Conference on Learning Representations*, 2023.
- [35] George Sugihara, Robert May, Hao Ye, Chih-hao Hsieh, Ethan Deyle, Michael Fogarty, and Stephan Munch. Detecting causality in complex ecosystems. *Science*, 338(6106):496–500, 2012.
- [36] Elise Zhang, François Mirallès, Raphaël Rousseau-Rizzi, Di Wu, Arnaud Zinflou, and Benoit Boulet. Enhancing convergent cross mapping: Simple preprocessing for noise-resilient causal discovery. *Authorea Preprints*, 2024.
- [37] Gene Yu, Ce Guo, and Wayne Luk. Robust time series causal discovery for agent-based model validation. *arXiv preprint arXiv:2410.19412*, 2024.
- [38] Aapo Hyvärinen, Kun Zhang, Shohei Shimizu, and Patrik O Hoyer. Estimation of a structural vector autoregression model using non-gaussianity. *Journal of Machine Learning Research*, 11(5), 2010.
- [39] John Geweke. Measurement of linear dependence and feedback between multiple time series. *Journal of the American Statistical Association*, 77(378):304–313, 1982.
- [40] Jörg Breitung and Bertrand Candelon. Testing for short- and long-run causality: A frequency-domain approach. *Journal of Econometrics*, 132(2):363–378, 2006.
- [41] Gang-Jin Wang, Hui-Bin Si, Yang-Yang Chen, Chi Xie, and Julien Chevallier. Time domain and frequency domain granger causality networks: Application to china’s financial institutions. *Finance Research Letters*, 39:101662, 2021.
- [42] Richard Ashley and Randal J Verbrugge. Frequency dependence in regression model coefficients: an alternative approach for modeling nonlinear dynamic relationships in time series. *Econometric Reviews*, 28(1-3):4–20, 2008.

- [43] Debasish Maitra and Saumya Ranjan Dash. Sentiment and stock market volatility revisited: A time–frequency domain approach. *Journal of Behavioral and Experimental Finance*, 15:74–91, 2017.
- [44] George E. Uhlenbeck and Leonard S. Ornstein. On the theory of the brownian motion. *Physical Review*, 36(5):823–841, 1930.
- [45] Ross A Maller, Gernot Müller, and Alex Szimayer. Ornstein–uhlenbeck processes and extensions. *Handbook of financial time series*, pages 421–437, 2009.
- [46] Andrew Ang and Allan Timmermann. Regime changes and financial markets. *Annu. Rev. Financ. Econ.*, 4(1):313–337, 2012.
- [47] Wasim Ahmad, Maha Shadaydeh, and Joachim Denzler. Causal discovery using model invariance through knockoff interventions. In *ICML 2022 Workshop on Spurious Correlations, Invariance and Stability*, 2022.
- [48] Yizhou Cheng, Ziqian Wang, Tianyu Xiao, Qiu Zhong, Jiaqi Suo, and Kun He. Causalttime: Realistically generated time-series for benchmarking of causal discovery. In *The Twelfth International Conference on Learning Representations (ICLR)*, 2024.
- [49] David R. Brillinger. *Time Series: Data Analysis and Theory*. Holt, Rinehart and Winston, 2nd edition, 1981. Ch. 4.3.

A Theoretical Analysis

The proof of Theorem 1 is articulated in two main steps:

- (A) We first show that the feature sequence $(\mathbf{a}, \boldsymbol{\lambda})$ satisfies the classical assumptions required for valid inference using vector autoregressive (VAR) models, as established in [13].
- (B) We then demonstrate that the transformation \mathcal{T} , described in Algorithm 1, preserves the structure of the ground-truth causal graph \mathcal{G}^* , meaning that no spurious edges are introduced and no genuine dependencies are lost.

By combining these two results, we conclude that applying Granger causality analysis to the transformed sequence $(\mathbf{a}, \boldsymbol{\lambda})$ enables consistent recovery of the original causal graph \mathcal{G}^* .

In order to validate step (A), we decompose it into the following supporting claims:

- (A1) **Markovianity Preservation:** If the original process \mathbf{x} is a finite-order Markov process, then the derived features $(\mathbf{a}, \boldsymbol{\lambda})$ form a process with finite memory as well.
- (A2) **Weak Stationarity and Noise Assumptions:** The sequences $(\mathbf{a}, \boldsymbol{\lambda})$ are approximately weakly stationary and with an asymptotically Gaussian noise.
- (A3) **Preservation of Linear Dependence under Spectral Transformation:** The transformation \mathcal{T} , described in Algorithm 1, preserves linear relationships between corresponding time series. That is, if two time series are linearly dependent (e.g., one is a scalar multiple of the other), then their corresponding spectral features remain linearly dependent. Conversely, if the time series are not collinear in the time domain, their spectral representations will also be linearly independent.

Step (B) relies on just one structural condition:

- (B1) **Spectral Causality Preservation:** Causal relationships in the time domain induce systematic and detectable dependencies among the corresponding spectral features.

Steps (A1) and (A2) establish the two key requirements needed to apply a VAR analysis for studying Granger causality.

In particular, Theorem 2 provides the proof that Markovianity is preserved for the transformed features $(\mathbf{a}, \boldsymbol{\lambda})$, that is the claim of (A1).

Theorem 3 discusses the assumptions of weak stationarity and Gaussianity of the noise. It shows that the procedure \mathcal{T} , described in Algorithm 1, transforms any colored noise affecting \mathbf{x} into an asymptotically Gaussian noise on $(\mathbf{a}, \boldsymbol{\lambda})$. This proves step (A2). Moreover, some of the strong assumptions of Theorem 3 are dropped in Theorem 4, which shows that, under additional assumptions on the time series beyond the power-law behavior, the weak stationarity of the $\boldsymbol{\lambda}$ parameter is preserved even in certain cases where \mathbf{x} itself is non-stationary. Notably, the synthetic datasets described in Section 5.1 fall in this scenario.

Theorem 5 addresses the component (A3), proving the preservation of linear dependencies under the transformation \mathcal{T} .

Finally, Theorem 6 concludes the proof showing that causal relationships are preserved in the transformed time series $(\mathbf{a}, \boldsymbol{\lambda})$ (B1).

(A1) Markovianity Preservation

Theorem 2 (Markovianity of Spectral Features Derived from a Markov Process). *Let $\mathbf{x} = \{x(t)\}$ be a time series following a Markov process of order p . Let the spectral features $(\mathbf{a}, \boldsymbol{\lambda})$ be obtained via the transformation \mathcal{T} , described in Algorithm 1, applied to a window of length l and stride $s < l$, acting locally on \mathbf{x} . Then, the resulting feature sequence $(\mathbf{a}, \boldsymbol{\lambda})$ is a finite-order Markov process of order p' satisfying:*

$$p' = \left\lfloor \frac{p-l}{s} \right\rfloor + 1. \quad (4)$$

Proof. By hypothesis, the process \mathbf{x} satisfies the following equation:

$$\mathbb{P}[x(t) \mid x(t-1), x(t-2), \dots] = \mathbb{P}[x(t) \mid x(t-1), \dots, x(t-p)].$$

For each time window k , the spectral features (a^k, λ^k) are obtained as in Algorithm 1. The last element of the time series in window k is $x(ks + l - 1)$. The entire window W_k spans from time ks to $ks + l - 1$.

To reconstruct the Markov state at time t , we need enough windows such that their union contains the entire interval $[t - p + 1, t]$.

Let p' be the minimum number of windows to cover p time steps of the process. It must hold that:

$$(p' - 1) \cdot s + l \geq p.$$

Solving for p' gives:

$$p' = \left\lfloor \frac{p - l}{s} \right\rfloor + 1.$$

Therefore, the feature sequence $(\mathbf{a}, \boldsymbol{\lambda})$ is itself a Markov process of order $p' < p$. \square

(A2) Weak Stationarity and Noise Assumptions

Theorem 3 (Asymptotic Gaussianity and Stationarity under Colored Noise). *Let $\mathbf{x} = \{x(t)\}$ be a weakly stationary process with power spectral density $S(f_k) \propto 1/f_k^\alpha$ for $\alpha \geq 0$, where f_k denotes the k -th frequency component. Let $\phi(k)$ be the DFT over a window of size l , and define $(\mathbf{a}, \boldsymbol{\lambda})$ as in Algorithm 1. Then, for sufficiently large l , the sequences $(\mathbf{a}, \boldsymbol{\lambda})$ are approximately Gaussian and weakly stationary.*

Proof. As shown in [49], if \mathbf{x} is a weakly stationary process with decaying autocorrelation, then the Discrete Fourier Transform (DFT) coefficients computed over a window of size l converge in distribution to complex Gaussian variables with variance given by the power spectral density $S(f_k)$. That is,

$$\phi_k \xrightarrow{d} \mathcal{CN}(0, S(f_k)).$$

The spectral amplitudes $A_k = |\phi_k|$ follow a Rayleigh distribution with scale parameter determined by $S(f_k)$. Let $(\mathbf{a}, \boldsymbol{\lambda})$ be computed as in Algorithm 1, by linear regression on the pairs $(\log f_k, \log A_k)$ within each window. Although the $\log A_k$ are not Gaussian, the regression combines information from many such values. Since the estimators are linear combinations of independent (or weakly dependent) inputs with finite variance, they are approximately Gaussian by the Central Limit Theorem.

Therefore, for sufficiently large window length l , the estimated features $(\mathbf{a}, \boldsymbol{\lambda})$ can be treated as approximately Gaussian variables.

Regarding the i.i.d. assumption of the noise, this trivially holds in the case of non-overlapping windows. However, when the windows overlap, the input data for consecutive Fourier transforms share common segments, which induces statistical dependence between the resulting spectral estimates. As a consequence, the noise affecting the estimated parameters $(\mathbf{a}, \boldsymbol{\lambda})$ is not independent across windows, but exhibits weak temporal correlation. \square

Theorem 4 (Stationarity of Intercept Sequence for Certain Non-Stationary Processes). *Let \mathbf{x} be a power-law time series. Let us assume that the following equivalence holds:*

$$\mathbb{E}[x(t)] \propto \mathbb{E}[x(t - \tau)],$$

for all t and shifts τ . Let $A^k(f) = |\phi_k(f)|$ denote the local Fourier amplitude of \mathbf{x} over window k , and assume \mathbf{x} has a power-law spectrum.

Then the sequence $\boldsymbol{\lambda} = \{\lambda_k\}$ as in Algorithm 1 is weakly stationary.

Proof. Let us call $\mathbf{w}^k = (x(k \cdot l), \dots, x((k + 1) \cdot l - 1))$, and $\mathbf{w}^{k-\tau} = (x(k \cdot l - \tau), \dots, x((k + 1) \cdot l - 1 - \tau))$, for each window k . By hypothesis, it follows that for each k , $\exists b^k$ such that

$$\mathbb{E}[\mathbf{w}^k] = b^k \cdot \mathbb{E}[\mathbf{w}^{k-\tau}].$$

Now consider the discrete Fourier transform in window k :

$$\mathbb{E}[\phi_k(f)] = \mathbb{E}[\mathcal{F}[\mathbf{w}^k]].$$

Let $\phi_{k-\tau}(f) = \mathcal{F}(\mathbf{w}^{k-\tau})$. Since the Fourier transform is a linear operator, we have:

$$\mathbb{E}[\phi_k(f)] = b^k \cdot \mathbb{E}[\phi_{k-\tau}(f)],$$

and consequently:

$$\mathbb{E}[A^k(f)] = \mathbb{E}[|\phi_k(f)|] = b^k \cdot \mathbb{E}[|\phi_{k-\tau}(f)|] = b^k \cdot \mathbb{E}[A^{k-\tau}(f)],$$

where $A^{k-\tau} = |\phi_{k-\tau}(f)|$.

Taking logarithms of the amplitude:

$$\mathbb{E}[\log A^k(f)] = \mathbb{E}[\log A^{k-\tau}(f)] + \log b^k.$$

Assuming that $A^{k-\tau}(f)$ follows a log-log linear form, it follows that:

$$\mathbb{E}[\log A^{k-\tau}(f)] = -\mathbb{E}[\lambda_{k-\tau}] \log f + \mathbb{E}[a_{k-\tau}],$$

where $\lambda_{k-\tau}$ and $a_{k-\tau}$ are the parameters fitted on the window $\mathbf{w}^{k-\tau}$ as in Algorithm 1. Then:

$$\mathbb{E}[\log A^k(f)] = -\mathbb{E}[\lambda_{k-\tau}] \log f + \mathbb{E}[a_{k-\tau}] + \log b^k.$$

From the last formula, it results that the dynamics of the mean of λ is not impacted by the scaling parameter b^k . Furthermore, assuming the invariance of the second moment of the original time series under translations, one obtains that the spectral slope time series is weakly stationarity. \square

(A3) Preservation of Linear Dependence under Spectral Transformation

Theorem 5 (Preservation of Linear Dependence under Spectral Transformation). *Let \mathbf{x}_i and \mathbf{x}_j be two power-law time series and \mathcal{T} the transformation described in Algorithm 1.*

Then:

- *If $\mathbf{x}_j = \alpha \cdot \mathbf{x}_i$ for some constant $\alpha \in \mathbb{R}$ and all t , then $\lambda_j = \lambda_i$ and $\mathbf{a}_j = \mathbf{a}_i + \log |\alpha|$.*
- *If \mathbf{x}_i and \mathbf{x}_j are not perfectly collinear in the time domain, then $(\mathbf{a}_i, \lambda_i)$ and $(\mathbf{a}_j, \lambda_j)$ are not collinear in the feature domain either.*

Therefore, the spectral transformation \mathcal{T} preserves both linear dependence and linear independence between time series.

Proof. The following proof is divided in two cases:

Case 1: Collinearity. Suppose $\mathbf{x}_j = \alpha \cdot \mathbf{x}_i$. Then, the power spectra satisfy:

$$A_j(f) = |\mathcal{F}[\mathbf{x}_j]| = |\alpha \cdot \mathcal{F}[\mathbf{x}_i]| = |\alpha| \cdot A_i(f),$$

which implies:

$$\log A_j(f) = \log A_i(f) + \log |\alpha|,$$

and so $\forall f$,

$$-\lambda_j \log f + \mathbf{a}_j = -\lambda_i \log f + \mathbf{a}_i + \log |\alpha|.$$

Therefore, both series have the same spectral slope

$$\lambda_j = \lambda_i,$$

and the intercepts differ by a constant:

$$\mathbf{a}_j(t) = \mathbf{a}_i(t) + \log |\alpha|.$$

Hence, \mathcal{T} preserves both linear dependence between λ_i and λ_j .

Case 2: Non-collinearity. Assume that \mathbf{x}_i and \mathbf{x}_j are not linearly dependent. Then, their power spectra must differ in structure, i.e $\log A_i(f)$ and $\log A_j(f)$ cannot have the same slope across frequencies.

Hence, the fit of the λ_i and λ_j parameters of \mathcal{T} preserves independence between them. \square

(B1) Spectral Causality Preservation

Theorem 6 (Preservation of Causal Structure under Spectral Transformation). *Let \mathbf{x}_i and \mathbf{x}_j be two power-law time series such that*

$$\mathbf{x}_i = g(\mathbf{x}_j) + \boldsymbol{\eta}, \quad (5)$$

where g is a function and $\boldsymbol{\eta} = \{\eta(t)\}$ is additive noise independent of \mathbf{x}_j . Then, the spectral parameters $(\mathbf{a}_i, \boldsymbol{\lambda}_i)$ defined in Algorithm 1 retain information about the causal influence from \mathbf{x}_j to \mathbf{x}_i .

Proof. Applying the Fourier transform to both sides of Equation (5) and exploiting the linearity of the Fourier transform, we get:

$$\mathcal{F}[(\mathbf{x}_i)] = \mathcal{F}[g(\mathbf{x}_j)] + \mathcal{F}[\boldsymbol{\eta}].$$

We prove that in both linear and nonlinear settings, the spectral amplitude $A_i(f)$ retains features shaped by the causal dependency on \mathbf{x}_j . Consequently, the pair $(\mathbf{a}_i, \boldsymbol{\lambda}_i)$ derived from a log-log fit of $A_i(f)$ preserves causal information.

Case 1: g is linear. If g is a linear operator, then by the linearity of \mathcal{F} ,

$$\mathcal{F}[g(\mathbf{x}_j)] = g(\mathcal{F}[\mathbf{x}_j]).$$

Taking the modulus yields:

$$A_i(f) = |g(A_j(f))| + \mathcal{F}[\boldsymbol{\eta}].$$

If $A_j(f) \propto f^{-\lambda_j}$ (i.e., \mathbf{x}_j exhibits a power-law spectrum), then under mild regularity assumptions on g , the transformed amplitude $A_i(f)$ also exhibits a power-law decay:

$$A_i(f) \propto f^{-\lambda_i}, \quad \text{with } \lambda_i = \lambda_j + \Delta\lambda,$$

where $\Delta\lambda$ captures the spectral effect of g . Thus, the spectral slope λ_i contains information induced by the causal transformation g .

Case 2: g is nonlinear. For nonlinear g , $\mathcal{F}[g(\mathbf{x}_j)] \neq g(\mathcal{F}[\mathbf{x}_j])$ in general. However, due to the orthogonality and completeness of the Fourier basis, the operation g induces structured interactions among frequencies. This distorts but does not destroy the underlying spectral shape.

Hence, even under nonlinear transformations, the global decay behavior captured by the spectral parameters $\boldsymbol{\lambda}$ remains a meaningful summary of the causal influence. \square

B Mathematical computation of λ for our Synthetic Datasets

In this section, we provide a mathematical derivation of the spectral parameter λ for the linear additive system used to generate the synthetic datasets in Section 5.1.

Let \mathbf{x}_1 , \mathbf{x}_2 , and \mathbf{x}_3 be three time series whose spectral amplitudes follow a power-law profile. In the case of an additive interaction in the time domain, the resulting spectral amplitude of \mathbf{x}_1 can be expressed—under idealized linearity and independence assumptions—as:

$$\forall f \quad A_1(f) = A_2(f) + c \cdot A_3(f)$$

where c is a scalar coefficient regulating the strength of the contribution from \mathbf{x}_3 to \mathbf{x}_1 , and f the value of a frequency of the spectrum.

$$A_1(f) = e^{\mathbf{a}_1} \cdot f^{-\lambda_1}, \quad A_2(f) = e^{\mathbf{a}_2} \cdot f^{-\lambda_2}, \quad A_3(f) = e^{\mathbf{a}_3} \cdot f^{-\lambda_3}$$

Substituting into the first equation gives:

$$e^{\mathbf{a}_1} \cdot f^{-\lambda_1} = e^{\mathbf{a}_2} \cdot f^{-\lambda_2} + c \cdot e^{\mathbf{a}_3} \cdot f^{-\lambda_3} \quad (6)$$

Case 1: Assume the following:

$$\frac{c \cdot e^{\mathbf{a}_3}}{e^{\mathbf{a}_2}} \cdot f^{\lambda_2 - \lambda_3} \gg 1. \quad (7)$$

Notice that we can write the right-hand side of Equation (6) as $e^{\mathbf{a}_2} \cdot f^{-\lambda_2} \left[1 + \frac{c \cdot e^{\mathbf{a}_3}}{e^{\mathbf{a}_2}} \cdot f^{\lambda_2 - \lambda_3} \right]$. By applying this substitution, taking the natural logarithm in Equation (6), and using logarithmic properties, we get:

$$\log(e^{\mathbf{a}_1} \cdot f^{-\lambda_1}) = \log\left(e^{\mathbf{a}_2} \cdot f^{-\lambda_2} \left[1 + \frac{c \cdot e^{\mathbf{a}_3}}{e^{\mathbf{a}_2}} \cdot f^{\lambda_2 - \lambda_3} \right]\right) \quad (8)$$

$$= \mathbf{a}_2 - \lambda_2 \log f + \log\left(1 + \frac{c \cdot e^{\mathbf{a}_3}}{e^{\mathbf{a}_2}} \cdot f^{\lambda_2 - \lambda_3}\right) \quad (9)$$

Given the assumption in Equation (7), the logarithmic term in the previous equation can be approximated as:

$$\log\left(1 + \frac{c \cdot e^{\mathbf{a}_3}}{e^{\mathbf{a}_2}} \cdot f^{\lambda_2 - \lambda_3}\right) \approx \log\left(\frac{c \cdot e^{\mathbf{a}_3}}{e^{\mathbf{a}_2}} \cdot f^{\lambda_2 - \lambda_3}\right)$$

By substituting this expression in Equation (8), we obtain the following equation:

$$\mathbf{a}_1 - \lambda_1 \log f \approx \mathbf{a}_2 - \lambda_2 \log f + \log\left(\frac{c \cdot e^{\mathbf{a}_3}}{e^{\mathbf{a}_2}}\right) + (\lambda_2 - \lambda_3) \log f$$

Which can be simplified as follows:

$$\mathbf{a}_1 - \lambda_1 \log f \approx \log c + \mathbf{a}_3 - \lambda_3 \log f$$

Finally, by solving for λ_1 , we get the following expression for λ_1 :

$$\lambda_1 \approx \lambda_3 + \frac{\log c + \mathbf{a}_3 - \mathbf{a}_1}{\log f}$$

This shows that the spectral decay parameter λ_1 approximates λ_3 with a correction term depending on the scaling factor c , the spectral amplitude, and frequency.

Case 2: Now consider the case where $\frac{c \cdot e^{\mathbf{a}_3}}{e^{\mathbf{a}_2}} \cdot f^{\lambda_2 - \lambda_3} \ll 1$, such as when $c \rightarrow 0$. The logarithmic term is approximated using the first-order Taylor expansion:

$$\log\left(1 + \frac{c \cdot e^{\mathbf{a}_3}}{e^{\mathbf{a}_2}} \cdot f^{\lambda_2 - \lambda_3}\right) \approx \frac{c \cdot e^{\mathbf{a}_3}}{e^{\mathbf{a}_2}} \cdot f^{\lambda_2 - \lambda_3}$$

Substituting into the main expression:

$$\mathbf{a}_1 - \lambda_1 \log f \approx \mathbf{a}_2 - \lambda_2 \log f + \frac{c \cdot e^{\mathbf{a}_3}}{e^{\mathbf{a}_2}} \cdot f^{\lambda_2 - \lambda_3}$$

Solving for λ_1 :

$$\lambda_1 \approx \lambda_2 + \frac{\mathbf{a}_2 - \mathbf{a}_1}{\log f} + c \cdot e^{\mathbf{a}_3 - \mathbf{a}_2} \cdot \frac{f^{\lambda_2 - \lambda_3}}{\log f}$$

As $c \rightarrow 0$, the correction vanishes, and $\lambda_1 \rightarrow \lambda_2$, showing that the spectrum of the target converges to that of the source.

C Discussion on the VAR Inputs

From the expressions derived in Appendix B, it becomes evident that in the linear case one can identify certain quantities that are valuable inputs to a VAR model. As an example, given the two time series x_1 and x_3 of Appendix B, the relevant quantities are:

- a_1 : spectral intercept of the caused time series
- a_3 : spectral intercept of the causing time series
- λ_1 : spectral slope of the caused time series
- λ_3 : spectral slope of the causing time series

In this analysis, we neglect higher-order terms (e.g., exponentials in a), as they empirically fail to improve system performance and are not present in the asymptotic regime discussed in Appendix B.

Each time series thus provides two spectral parameters: λ and a . Among these, the λ parameters are identified as the main carriers of causal information. The simplest model we can consider involves assessing Granger causality between the λ sequences, i.e., testing for $\lambda_3 \rightarrow \lambda_1$ relationships.

To enhance the system's robustness in the presence of stationary processes, including the a parameter as a covariate in the VAR model has shown some performance improvements. However, in non-stationary settings, adding the a provides no additional causal information beyond λ .

Finally, using the a parameter of the caused series either as an input or as a target in the VAR model has proven ineffective: while it does not meaningfully improve performance in the stationary case, it introduces false positives in non-stationary regimes. Therefore, its inclusion is not theoretically nor empirically justified.

C.1 Study of p -values for Setting Window Length and Stride

In the proposed framework, both the stride and the sliding window length are configurable parameters that can be tuned by the user. The stride primarily serves to increase the number of available data points for analysis and plays a crucial role in the system's ability to detect short-range causal dependencies. If the true causal lag is shorter than the selected stride, the system may fail to capture such dynamics. Therefore, it is generally recommended to set the stride to 1. The sliding window length is a more delicate parameter, as it is influenced by multiple factors. A window that is too short may yield unreliable estimates due to limited data, whereas an excessively long window may blur or attenuate the causal signal, thus reducing detection sensitivity. To mitigate this trade-off, we introduce a data-driven procedure to estimate a suitable window length. This involves a preliminary evaluation of the fitting procedure across various window sizes, based on the distribution of p -values over the entire spectrum. The smallest window size that satisfies a p -value of 0.05 is then selected for subsequent causal inference.

A reasonable requirement is also to fix a lower bound of this experimental criterion to a window length of a minimum of 50 datapoints. A smaller window may still satisfy the p -value requirement, but it will also make the fitted λ parameter too sensitive to endogenous variation of the autocorrelation caused by the phenomenon.

C.2 Slow-Varying Spectrum Systems

There are cases in which the system is sampled at such a high rate that it exhibits minimal local spectral variation. This typically occurs when the white noise component is small compared to other system dynamics. In these scenarios, spectral analysis becomes challenging, as we rely on observing how the spectrum evolves over time to infer causal relationships.

To address this issue, one should increase the window length and, if possible, reduce the stride of the sliding window. This allows the VAR model in the frequency domain to capture meaningful variations in the time series and better estimate potential causal links.

In these situations, time-domain methods like Granger causality may be more appropriate. While this introduces a limitation, the selection of a suitable causal inference technique can be effectively informed by an initial spectral analysis.

D Further Experimental Details and Results

D.1 OU Processes

Figure 3 shows two examples of the simulated OU processes, and the related causal graphs. In particular, an example of $\text{OU}(\sigma_g^m = 0)$ is shown in Figure 3a and an example of $\text{OU}(\sigma_g^m > 0)$ is shown in Figure 3b.

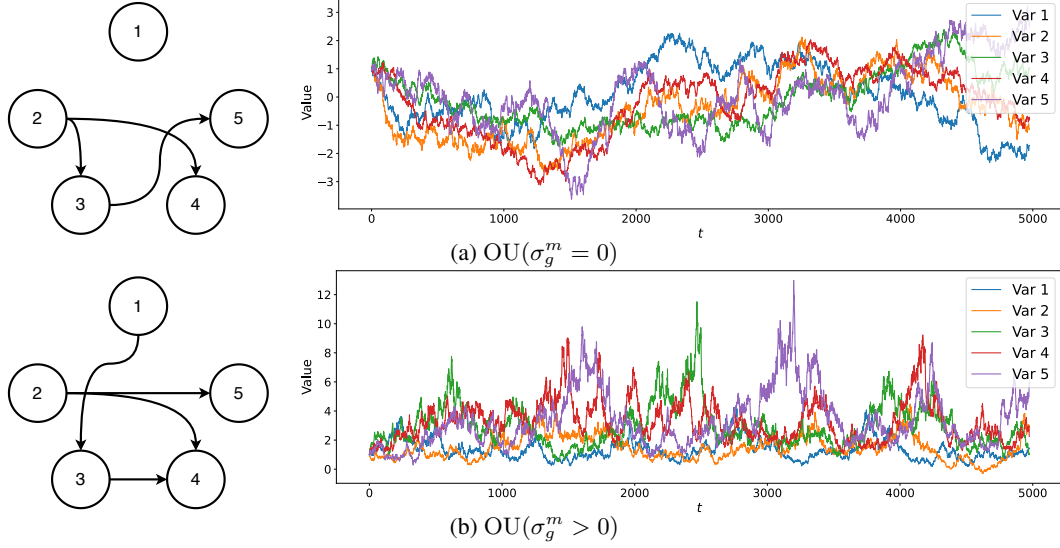


Figure 3: Generated synthetic processes.

D.2 Hyper-Parameters

Table 3 shows the list of the hyper-parameters that we set for each causal discovery algorithm. Wherever possible, we adopted the hyper-parameters specified in the original papers, adjusting them only in cases of extremely slow computation or lack of algorithmic convergence.

Table 3: Hyper-parameters of the causal discovery algorithms.

Algorithm	Hyper-Parameter	Value
Granger	maxlag	10
	p-value	0.05
PLaCy	window length (l)	50
	stride (s)	1
	p-value	0.05
PCMCi	τ_{max}	10
	Conditional Independence Test	Partial Correlation
	PC_α	0.05
CCM-Filtering	Filter Size	5
	Stride	1
	τ	10
	L	range(25, L , 250)
RCV-VarLiNGAM	k	7
	Sequence Length	300
	τ_c	0.7
	τ_v	0.4
Rhino	Noise Distribution	Gaussian
	init_rho	30
	init_alpha	0.2
DYNOTEARS	p	10
	max_iter	100
PCMCi $_\Omega$	τ_{max}	10

D.3 Additional Results

Tables 4 to 7 present all the experimental results for different configurations. We analyze the impact of varying the number of variables ($N \in \{5, 10\}$) and the scaling factor $\sigma_g^a \in \{0.5, 1\}$ on the methods' performance.

Table 4: F1 Score - $N = 5$, $\sigma_g^a = 1.0$

Dataset	C	σ_b	Granger	PLACy	PCMCI	CCM-Filtering	RCV-VarLiNGAM	Rhino	DYNOTEARS	PCMCI $_{\Omega}$
$\text{OU}(\sigma_g^m = 0)$	0.2	0.0	0.85 ± 0.20	0.13 ± 0.21	0.08 ± 0.19	0.11 ± 0.17	0.44 ± 0.17	0.24 ± 0.11	0.05 ± 0.16	0.06 ± 0.12
		0.1	0.63 ± 0.21	0.14 ± 0.21	0.06 ± 0.14	0.14 ± 0.19	0.43 ± 0.17	0.14 ± 0.11	0.15 ± 0.21	0.04 ± 0.11
		0.5	0.43 ± 0.17	0.13 ± 0.21	0.22 ± 0.28	0.23 ± 0.16	0.36 ± 0.19	0.13 ± 0.11	0.23 ± 0.15	0.10 ± 0.13
		1.0	0.39 ± 0.14	0.15 ± 0.24	0.24 ± 0.26	0.25 ± 0.15	0.36 ± 0.21	0.17 ± 0.14	0.23 ± 0.13	0.10 ± 0.14
	0.5	0.0	0.82 ± 0.19	0.83 ± 0.16	0.08 ± 0.19	0.10 ± 0.16	0.44 ± 0.18	0.34 ± 0.17	0.02 ± 0.12	0.08 ± 0.12
		0.1	0.62 ± 0.22	0.81 ± 0.19	0.07 ± 0.17	0.19 ± 0.20	0.43 ± 0.16	0.13 ± 0.12	0.02 ± 0.09	0.08 ± 0.12
		0.5	0.43 ± 0.16	0.67 ± 0.28	0.34 ± 0.27	0.22 ± 0.15	0.37 ± 0.19	0.18 ± 0.14	0.12 ± 0.20	0.11 ± 0.15
		1.0	0.37 ± 0.13	0.60 ± 0.25	0.32 ± 0.27	0.24 ± 0.15	0.33 ± 0.19	0.11 ± 0.10	0.16 ± 0.22	0.18 ± 0.16
	1.0	0.0	0.78 ± 0.20	0.78 ± 0.15	0.19 ± 0.27	0.20 ± 0.21	0.40 ± 0.17	0.32 ± 0.12	0.02 ± 0.09	0.08 ± 0.13
		0.1	0.61 ± 0.21	0.77 ± 0.18	0.15 ± 0.25	0.26 ± 0.22	0.39 ± 0.17	0.29 ± 0.15	0.04 ± 0.13	0.09 ± 0.13
		0.5	0.39 ± 0.16	0.78 ± 0.17	0.38 ± 0.29	0.26 ± 0.15	0.27 ± 0.22	0.20 ± 0.14	0.12 ± 0.18	0.15 ± 0.16
		1.0	0.35 ± 0.12	0.73 ± 0.19	0.37 ± 0.27	0.27 ± 0.15	0.22 ± 0.20	0.27 ± 0.11	0.14 ± 0.22	0.20 ± 0.16
$\widetilde{\text{OU}}(\sigma_g^m = 0)$	0.2	0.0	0.85 ± 0.19	0.21 ± 0.24	0.06 ± 0.18	0.26 ± 0.11	0.44 ± 0.17	0.12 ± 0.16	0.00 ± 0.00	0.06 ± 0.12
		0.1	0.47 ± 0.19	0.34 ± 0.24	0.04 ± 0.13	0.26 ± 0.11	0.44 ± 0.17	0.17 ± 0.15	0.00 ± 0.00	0.06 ± 0.12
		0.5	0.27 ± 0.11	0.22 ± 0.24	0.31 ± 0.27	0.25 ± 0.12	0.38 ± 0.19	0.23 ± 0.07	0.02 ± 0.12	0.09 ± 0.13
		1.0	0.28 ± 0.11	0.19 ± 0.24	0.24 ± 0.26	0.26 ± 0.14	0.38 ± 0.20	0.22 ± 0.11	0.05 ± 0.16	0.09 ± 0.13
	0.5	0.0	0.81 ± 0.19	0.79 ± 0.18	0.10 ± 0.19	0.26 ± 0.11	0.43 ± 0.17	0.12 ± 0.12	0.00 ± 0.00	0.08 ± 0.12
		0.1	0.45 ± 0.18	0.71 ± 0.18	0.06 ± 0.15	0.26 ± 0.11	0.43 ± 0.17	0.26 ± 0.11	0.00 ± 0.00	0.07 ± 0.12
		0.5	0.26 ± 0.11	0.70 ± 0.22	0.39 ± 0.25	0.25 ± 0.12	0.32 ± 0.20	0.27 ± 0.12	0.00 ± 0.04	0.09 ± 0.15
		1.0	0.28 ± 0.11	0.56 ± 0.25	0.31 ± 0.26	0.25 ± 0.13	0.30 ± 0.22	0.22 ± 0.08	0.02 ± 0.10	0.16 ± 0.16
	1.0	0.0	0.78 ± 0.19	0.74 ± 0.18	0.18 ± 0.25	0.26 ± 0.11	0.37 ± 0.17	0.29 ± 0.11	0.00 ± 0.00	0.08 ± 0.13
		0.1	0.46 ± 0.19	0.68 ± 0.17	0.12 ± 0.21	0.26 ± 0.11	0.37 ± 0.17	0.28 ± 0.10	0.00 ± 0.00	0.08 ± 0.13
		0.5	0.27 ± 0.11	0.71 ± 0.16	0.45 ± 0.27	0.27 ± 0.12	0.29 ± 0.20	0.27 ± 0.12	0.01 ± 0.05	0.11 ± 0.13
		1.0	0.28 ± 0.11	0.66 ± 0.17	0.42 ± 0.30	0.27 ± 0.13	0.25 ± 0.20	0.23 ± 0.13	0.02 ± 0.10	0.23 ± 0.17
$\text{OU}(\sigma_g^m > 0)$	0.2	0.0	0.65 ± 0.22	0.68 ± 0.25	0.25 ± 0.31	0.19 ± 0.22	0.41 ± 0.19	0.39 ± 0.22	0.20 ± 0.16	0.16 ± 0.16
		0.1	0.64 ± 0.22	0.70 ± 0.25	0.25 ± 0.30	0.17 ± 0.20	0.39 ± 0.18	0.32 ± 0.20	0.18 ± 0.16	0.15 ± 0.16
		0.5	0.64 ± 0.19	0.71 ± 0.24	0.23 ± 0.28	0.22 ± 0.21	0.37 ± 0.18	0.34 ± 0.17	0.24 ± 0.12	0.17 ± 0.17
		1.0	0.59 ± 0.21	0.79 ± 0.22	0.21 ± 0.27	0.16 ± 0.19	0.38 ± 0.18	0.40 ± 0.16	0.26 ± 0.11	0.15 ± 0.16
	0.5	0.0	0.61 ± 0.19	0.82 ± 0.17	0.41 ± 0.34	0.20 ± 0.20	0.35 ± 0.19	0.43 ± 0.23	0.09 ± 0.17	0.20 ± 0.16
		0.1	0.64 ± 0.19	0.76 ± 0.18	0.42 ± 0.32	0.20 ± 0.22	0.34 ± 0.19	0.50 ± 0.20	0.09 ± 0.17	0.23 ± 0.17
		0.5	0.61 ± 0.20	0.80 ± 0.16	0.43 ± 0.32	0.21 ± 0.19	0.32 ± 0.21	0.54 ± 0.12	0.20 ± 0.16	0.22 ± 0.16
		1.0	0.61 ± 0.21	0.80 ± 0.16	0.37 ± 0.32	0.19 ± 0.20	0.33 ± 0.22	0.46 ± 0.09	0.21 ± 0.14	0.22 ± 0.16
	1.0	0.0	0.57 ± 0.18	0.78 ± 0.18	0.62 ± 0.28	0.28 ± 0.21	0.32 ± 0.20	0.54 ± 0.14	0.11 ± 0.17	0.22 ± 0.16
		0.1	0.57 ± 0.18	0.76 ± 0.18	0.61 ± 0.29	0.22 ± 0.20	0.28 ± 0.21	0.52 ± 0.12	0.13 ± 0.19	0.21 ± 0.17
		0.5	0.56 ± 0.19	0.76 ± 0.17	0.55 ± 0.32	0.25 ± 0.20	0.25 ± 0.21	0.48 ± 0.12	0.23 ± 0.17	0.24 ± 0.18
		1.0	0.58 ± 0.19	0.77 ± 0.19	0.60 ± 0.29	0.29 ± 0.21	0.28 ± 0.21	0.46 ± 0.08	0.23 ± 0.16	0.25 ± 0.19
$\widetilde{\text{OU}}(\sigma_g^m > 0)$	0.2	0.0	0.29 ± 0.12	0.74 ± 0.21	0.37 ± 0.24	0.27 ± 0.14	0.12 ± 0.21	0.08 ± 0.15	0.02 ± 0.08	0.25 ± 0.12
		0.1	0.30 ± 0.12	0.74 ± 0.21	0.36 ± 0.24	0.26 ± 0.14	0.12 ± 0.20	0.14 ± 0.16	0.03 ± 0.13	0.26 ± 0.12
		0.5	0.43 ± 0.19	0.77 ± 0.20	0.31 ± 0.26	0.26 ± 0.19	0.28 ± 0.22	0.23 ± 0.21	0.02 ± 0.07	0.19 ± 0.14
		1.0	0.54 ± 0.22	0.77 ± 0.23	0.25 ± 0.30	0.19 ± 0.20	0.35 ± 0.18	0.26 ± 0.17	0.02 ± 0.10	0.17 ± 0.15
	0.5	0.0	0.29 ± 0.12	0.82 ± 0.16	0.46 ± 0.20	0.29 ± 0.13	0.07 ± 0.16	0.21 ± 0.24	0.01 ± 0.06	0.26 ± 0.11
		0.1	0.31 ± 0.12	0.80 ± 0.17	0.46 ± 0.21	0.28 ± 0.16	0.11 ± 0.20	0.32 ± 0.15	0.01 ± 0.07	0.26 ± 0.12
		0.5	0.42 ± 0.16	0.80 ± 0.18	0.47 ± 0.28	0.26 ± 0.19	0.21 ± 0.20	0.39 ± 0.19	0.00 ± 0.03	0.22 ± 0.14
		1.0	0.53 ± 0.19	0.80 ± 0.18	0.44 ± 0.33	0.21 ± 0.19	0.29 ± 0.22	0.41 ± 0.24	0.01 ± 0.05	0.22 ± 0.15
	1.0	0.0	0.29 ± 0.11	0.78 ± 0.17	0.51 ± 0.21	0.30 ± 0.13	0.07 ± 0.15	0.37 ± 0.16	0.01 ± 0.05	0.27 ± 0.12
		0.1	0.30 ± 0.13	0.77 ± 0.17	0.52 ± 0.22	0.31 ± 0.14	0.09 ± 0.17	0.45 ± 0.18	0.02 ± 0.11	0.26 ± 0.13
		0.5	0.43 ± 0.17	0.77 ± 0.17	0.58 ± 0.26	0.30 ± 0.17	0.22 ± 0.22	0.42 ± 0.18	0.00 ± 0.03	0.25 ± 0.15
		1.0	0.52 ± 0.18	0.78 ± 0.17	0.60 ± 0.29	0.30 ± 0.19	0.22 ± 0.20	0.49 ± 0.12	0.01 ± 0.05	0.25 ± 0.18

Table 5: F1 Score - $N = 5$, $\sigma_g^a = 0.5$

Dataset	C	σ_b	Granger	PLACy	PCMCI	CCM-Filtering	RCV-VarLiNGAM	Rhino	DYNOTEARS	PCMCI $_{\Omega}$
$OU(\sigma_g^m = 0)$	0.2	0.0	0.85 ± 0.19	0.12 ± 0.19	0.06 ± 0.15	0.08 ± 0.15	0.44 ± 0.17	—	0.02 ± 0.11	0.06 ± 0.12
		0.1	0.44 ± 0.17	0.15 ± 0.22	0.09 ± 0.19	0.21 ± 0.20	0.44 ± 0.17	—	0.12 ± 0.21	0.08 ± 0.12
		0.5	0.40 ± 0.16	0.14 ± 0.19	0.24 ± 0.27	0.23 ± 0.14	0.36 ± 0.23	—	0.23 ± 0.13	0.10 ± 0.14
		1.0	0.49 ± 0.18	0.10 ± 0.18	0.11 ± 0.20	0.25 ± 0.14	0.34 ± 0.24	—	0.21 ± 0.13	0.14 ± 0.15
	0.5	0.0	0.82 ± 0.18	0.84 ± 0.17	0.11 ± 0.21	0.12 ± 0.17	0.44 ± 0.18	—	0.01 ± 0.10	0.06 ± 0.12
		0.1	0.43 ± 0.17	0.77 ± 0.23	0.13 ± 0.21	0.18 ± 0.20	0.41 ± 0.18	0.12 ± 0.12	0.02 ± 0.10	0.07 ± 0.11
		0.5	0.38 ± 0.14	0.60 ± 0.26	0.32 ± 0.27	0.23 ± 0.15	0.32 ± 0.24	—	0.10 ± 0.18	0.15 ± 0.16
		1.0	0.44 ± 0.14	0.41 ± 0.27	0.21 ± 0.27	0.23 ± 0.13	0.32 ± 0.23	—	0.11 ± 0.18	0.24 ± 0.17
	1.0	0.0	0.78 ± 0.19	0.78 ± 0.16	0.20 ± 0.28	0.24 ± 0.22	0.40 ± 0.17	—	0.01 ± 0.10	0.07 ± 0.13
		0.1	0.44 ± 0.18	0.77 ± 0.16	0.20 ± 0.26	0.25 ± 0.20	0.37 ± 0.18	—	0.04 ± 0.11	0.07 ± 0.11
		0.5	0.35 ± 0.12	0.74 ± 0.17	0.42 ± 0.28	0.26 ± 0.14	0.22 ± 0.21	—	0.17 ± 0.22	0.24 ± 0.17
		1.0	0.41 ± 0.13	0.65 ± 0.21	0.31 ± 0.28	0.26 ± 0.14	0.18 ± 0.22	—	0.18 ± 0.22	0.31 ± 0.16
$\widehat{OU}(\sigma_g^m = 0)$	0.2	0.0	0.85 ± 0.19	0.20 ± 0.24	0.06 ± 0.18	0.26 ± 0.11	0.44 ± 0.17	—	0.00 ± 0.00	0.06 ± 0.12
		0.1	0.33 ± 0.13	0.29 ± 0.23	0.16 ± 0.24	0.26 ± 0.10	0.42 ± 0.17	—	0.00 ± 0.00	0.05 ± 0.11
		0.5	0.27 ± 0.11	0.17 ± 0.22	0.29 ± 0.30	0.25 ± 0.12	0.38 ± 0.18	—	0.03 ± 0.12	0.12 ± 0.14
		1.0	0.36 ± 0.14	0.20 ± 0.23	0.15 ± 0.23	0.24 ± 0.12	0.33 ± 0.19	—	0.06 ± 0.15	0.14 ± 0.15
	0.5	0.0	0.81 ± 0.19	0.74 ± 0.17	0.09 ± 0.18	0.26 ± 0.11	0.44 ± 0.17	—	0.00 ± 0.00	0.08 ± 0.13
		0.1	0.32 ± 0.12	0.61 ± 0.20	0.17 ± 0.23	0.26 ± 0.11	0.42 ± 0.18	0.23 ± 0.11	0.00 ± 0.00	0.09 ± 0.13
		0.5	0.27 ± 0.11	0.57 ± 0.25	0.36 ± 0.28	0.25 ± 0.11	0.34 ± 0.22	—	0.01 ± 0.05	0.16 ± 0.15
		1.0	0.35 ± 0.12	0.46 ± 0.28	0.15 ± 0.24	0.25 ± 0.13	0.30 ± 0.21	—	0.03 ± 0.10	0.27 ± 0.18
	1.0	0.0	0.78 ± 0.19	0.71 ± 0.17	0.18 ± 0.25	0.26 ± 0.11	0.38 ± 0.17	—	0.00 ± 0.00	0.09 ± 0.13
		0.1	0.32 ± 0.12	0.58 ± 0.16	0.19 ± 0.26	0.26 ± 0.11	0.35 ± 0.17	—	0.00 ± 0.00	0.07 ± 0.12
		0.5	0.27 ± 0.11	0.65 ± 0.19	0.37 ± 0.28	0.27 ± 0.12	0.34 ± 0.22	—	0.01 ± 0.04	0.22 ± 0.17
		1.0	0.33 ± 0.12	0.60 ± 0.18	0.28 ± 0.29	0.26 ± 0.12	0.24 ± 0.23	—	0.03 ± 0.13	0.34 ± 0.17
$OU(\sigma_g^m > 0)$	0.2	0.0	0.74 ± 0.20	0.45 ± 0.31	0.14 ± 0.24	0.12 ± 0.18	0.45 ± 0.17	—	0.19 ± 0.16	0.14 ± 0.15
		0.1	0.68 ± 0.20	0.57 ± 0.29	0.11 ± 0.22	0.14 ± 0.18	0.41 ± 0.17	—	0.20 ± 0.19	0.11 ± 0.14
		0.5	0.66 ± 0.21	0.60 ± 0.29	0.11 ± 0.21	0.18 ± 0.20	0.40 ± 0.17	—	0.22 ± 0.13	0.14 ± 0.16
		1.0	0.69 ± 0.22	0.70 ± 0.20	0.08 ± 0.19	0.18 ± 0.20	0.43 ± 0.17	—	0.24 ± 0.12	0.13 ± 0.14
	0.5	0.0	0.70 ± 0.19	0.81 ± 0.14	0.24 ± 0.31	0.17 ± 0.20	0.42 ± 0.17	—	0.06 ± 0.16	0.16 ± 0.16
		0.1	0.66 ± 0.18	0.81 ± 0.19	0.26 ± 0.29	0.20 ± 0.21	0.40 ± 0.17	0.28 ± 0.13	0.04 ± 0.13	0.15 ± 0.16
		0.5	0.64 ± 0.19	0.77 ± 0.20	0.20 ± 0.26	0.17 ± 0.22	0.37 ± 0.19	—	0.13 ± 0.16	0.17 ± 0.17
		1.0	0.65 ± 0.19	0.80 ± 0.19	0.22 ± 0.29	0.20 ± 0.23	0.39 ± 0.19	—	0.14 ± 0.15	0.18 ± 0.16
	1.0	0.0	0.66 ± 0.19	0.78 ± 0.15	0.43 ± 0.34	0.28 ± 0.25	0.39 ± 0.18	—	0.07 ± 0.15	0.20 ± 0.17
		0.1	0.63 ± 0.19	0.77 ± 0.14	0.44 ± 0.34	0.19 ± 0.21	0.35 ± 0.17	—	0.03 ± 0.11	0.21 ± 0.19
		0.5	0.64 ± 0.18	0.78 ± 0.17	0.38 ± 0.34	0.26 ± 0.20	0.35 ± 0.20	—	0.13 ± 0.18	0.21 ± 0.18
		1.0	0.62 ± 0.20	0.74 ± 0.19	0.33 ± 0.34	0.26 ± 0.20	0.33 ± 0.21	—	0.15 ± 0.16	0.22 ± 0.16
$\widehat{OU}(\sigma_g^m > 0)$	0.2	0.0	0.27 ± 0.11	0.55 ± 0.31	0.35 ± 0.21	0.27 ± 0.12	0.09 ± 0.18	—	0.04 ± 0.14	0.26 ± 0.11
		0.1	0.27 ± 0.11	0.64 ± 0.28	0.36 ± 0.24	0.27 ± 0.12	0.11 ± 0.21	—	0.04 ± 0.14	0.26 ± 0.11
		0.5	0.38 ± 0.15	0.67 ± 0.25	0.23 ± 0.26	0.19 ± 0.16	0.35 ± 0.22	—	0.04 ± 0.12	0.22 ± 0.12
		1.0	0.56 ± 0.20	0.66 ± 0.27	0.14 ± 0.25	0.15 ± 0.16	0.42 ± 0.19	—	0.05 ± 0.16	0.14 ± 0.15
	0.5	0.0	0.27 ± 0.11	0.84 ± 0.14	0.45 ± 0.22	0.27 ± 0.11	0.06 ± 0.14	—	0.01 ± 0.08	0.26 ± 0.11
		0.1	0.27 ± 0.11	0.79 ± 0.18	0.44 ± 0.23	0.28 ± 0.12	0.08 ± 0.17	0.25 ± 0.18	0.01 ± 0.07	0.26 ± 0.11
		0.5	0.39 ± 0.15	0.79 ± 0.17	0.37 ± 0.29	0.26 ± 0.16	0.32 ± 0.21	—	0.01 ± 0.06	0.24 ± 0.14
		1.0	0.57 ± 0.19	0.82 ± 0.18	0.26 ± 0.30	0.21 ± 0.19	0.36 ± 0.20	—	0.01 ± 0.07	0.15 ± 0.15
	1.0	0.0	0.27 ± 0.11	0.80 ± 0.15	0.53 ± 0.21	0.28 ± 0.12	0.07 ± 0.16	—	0.02 ± 0.09	0.25 ± 0.11
		0.1	0.28 ± 0.11	0.81 ± 0.17	0.53 ± 0.21	0.28 ± 0.12	0.09 ± 0.20	—	0.02 ± 0.12	0.25 ± 0.12
		0.5	0.38 ± 0.16	0.76 ± 0.18	0.48 ± 0.30	0.28 ± 0.17	0.24 ± 0.21	—	0.02 ± 0.11	0.25 ± 0.14
		1.0	0.53 ± 0.18	0.78 ± 0.17	0.39 ± 0.32	0.27 ± 0.18	0.28 ± 0.21	—	0.03 ± 0.14	0.21 ± 0.15

Table 6: F1 Score - $N = 10$, $\sigma_g^a = 1.0$

Dataset	C	σ_b	Granger	PLACy	PCMCI	CCM-Filtering	RCV-VarLiNGAM	Rhino	DYNOTEARS	PCMCI $_{\Omega}$
$\text{OU}(\sigma_g^m = 0)$	0.2	0.0	0.88 ± 0.07	0.16 ± 0.11	0.06 ± 0.09	—	0.46 ± 0.08	—	0.08 ± 0.09	0.07 ± 0.06
		0.1	0.65 ± 0.10	0.17 ± 0.11	0.06 ± 0.08	—	0.46 ± 0.08	—	0.13 ± 0.09	0.07 ± 0.06
		0.5	0.46 ± 0.09	0.17 ± 0.11	0.20 ± 0.13	—	0.44 ± 0.08	—	0.21 ± 0.09	0.09 ± 0.06
		1.0	0.41 ± 0.07	0.16 ± 0.12	0.24 ± 0.12	—	0.41 ± 0.09	—	0.23 ± 0.09	0.11 ± 0.06
	0.5	0.0	0.67 ± 0.08	0.80 ± 0.07	0.16 ± 0.14	—	0.43 ± 0.08	—	0.03 ± 0.06	0.10 ± 0.06
		0.1	0.55 ± 0.08	0.79 ± 0.07	0.10 ± 0.11	—	0.43 ± 0.09	—	0.04 ± 0.07	0.10 ± 0.06
		0.5	0.39 ± 0.07	0.73 ± 0.07	0.28 ± 0.13	—	0.38 ± 0.09	0.22 ± 0.04	0.07 ± 0.09	0.12 ± 0.06
		1.0	0.36 ± 0.05	0.60 ± 0.11	0.27 ± 0.13	—	0.36 ± 0.11	—	0.07 ± 0.10	0.14 ± 0.06
	1.0	0.0	0.59 ± 0.09	0.59 ± 0.09	0.38 ± 0.19	—	0.38 ± 0.09	—	0.03 ± 0.07	0.12 ± 0.06
		0.1	0.53 ± 0.08	0.60 ± 0.09	0.24 ± 0.16	—	0.38 ± 0.08	—	0.05 ± 0.08	0.13 ± 0.06
		0.5	0.37 ± 0.06	0.59 ± 0.09	0.31 ± 0.13	—	0.31 ± 0.09	—	0.13 ± 0.13	0.14 ± 0.07
		1.0	0.34 ± 0.05	0.58 ± 0.09	0.30 ± 0.12	—	0.32 ± 0.10	—	0.14 ± 0.11	0.19 ± 0.07
$\widetilde{\text{OU}}(\sigma_g^m = 0)$	0.2	0.0	0.87 ± 0.07	0.24 ± 0.13	0.05 ± 0.08	—	0.45 ± 0.09	—	0.00 ± 0.00	0.07 ± 0.06
		0.1	0.49 ± 0.09	0.35 ± 0.11	0.07 ± 0.09	—	0.45 ± 0.08	—	0.00 ± 0.00	0.08 ± 0.06
		0.5	0.28 ± 0.05	0.25 ± 0.12	0.28 ± 0.12	—	0.44 ± 0.08	—	0.01 ± 0.03	0.09 ± 0.06
		1.0	0.29 ± 0.05	0.20 ± 0.10	0.25 ± 0.13	—	0.39 ± 0.09	—	0.04 ± 0.07	0.10 ± 0.06
	0.5	0.0	0.67 ± 0.07	0.75 ± 0.07	0.17 ± 0.13	—	0.43 ± 0.08	—	0.00 ± 0.00	0.10 ± 0.06
		0.1	0.43 ± 0.09	0.65 ± 0.06	0.10 ± 0.12	—	0.43 ± 0.09	—	0.00 ± 0.00	0.10 ± 0.06
		0.5	0.28 ± 0.05	0.69 ± 0.08	0.29 ± 0.12	—	0.38 ± 0.10	0.23 ± 0.05	0.00 ± 0.00	0.11 ± 0.07
		1.0	0.29 ± 0.05	0.59 ± 0.09	0.29 ± 0.14	—	0.34 ± 0.11	—	0.02 ± 0.04	0.14 ± 0.06
	1.0	0.0	0.59 ± 0.09	0.56 ± 0.08	0.38 ± 0.19	—	0.37 ± 0.08	—	0.00 ± 0.00	0.13 ± 0.06
		0.1	0.42 ± 0.08	0.51 ± 0.07	0.23 ± 0.17	—	0.36 ± 0.08	—	0.00 ± 0.00	0.14 ± 0.06
		0.5	0.28 ± 0.05	0.56 ± 0.08	0.30 ± 0.14	—	0.32 ± 0.09	—	0.01 ± 0.03	0.13 ± 0.07
		1.0	0.29 ± 0.05	0.54 ± 0.08	0.31 ± 0.12	—	0.29 ± 0.11	—	0.01 ± 0.03	0.19 ± 0.06
$\text{OU}(\sigma_g^m > 0)$	0.2	0.0	0.64 ± 0.11	0.69 ± 0.11	0.26 ± 0.16	—	0.43 ± 0.08	—	0.17 ± 0.09	0.15 ± 0.08
		0.1	0.61 ± 0.11	0.70 ± 0.10	0.32 ± 0.15	—	0.42 ± 0.08	—	0.18 ± 0.09	0.16 ± 0.07
		0.5	0.61 ± 0.10	0.73 ± 0.10	0.26 ± 0.15	—	0.41 ± 0.08	—	0.23 ± 0.07	0.17 ± 0.06
		1.0	0.60 ± 0.10	0.74 ± 0.09	0.28 ± 0.17	—	0.41 ± 0.08	—	0.23 ± 0.07	0.18 ± 0.08
	0.5	0.0	0.54 ± 0.10	0.69 ± 0.09	0.49 ± 0.17	—	0.39 ± 0.08	—	0.07 ± 0.09	0.19 ± 0.08
		0.1	0.54 ± 0.09	0.68 ± 0.08	0.47 ± 0.16	—	0.38 ± 0.09	—	0.09 ± 0.09	0.20 ± 0.07
		0.5	0.51 ± 0.10	0.66 ± 0.08	0.47 ± 0.15	—	0.34 ± 0.09	0.58 ± 0.05	0.15 ± 0.10	0.20 ± 0.08
		1.0	0.51 ± 0.11	0.67 ± 0.09	0.47 ± 0.14	—	0.35 ± 0.09	—	0.19 ± 0.09	0.20 ± 0.08
	1.0	0.0	0.47 ± 0.09	0.58 ± 0.08	0.63 ± 0.14	—	0.31 ± 0.09	—	0.07 ± 0.07	0.20 ± 0.07
		0.1	0.46 ± 0.09	0.58 ± 0.09	0.63 ± 0.12	—	0.28 ± 0.10	—	0.07 ± 0.08	0.22 ± 0.07
		0.5	0.46 ± 0.08	0.58 ± 0.09	0.61 ± 0.12	—	0.27 ± 0.11	—	0.15 ± 0.09	0.23 ± 0.06
		1.0	0.44 ± 0.08	0.58 ± 0.10	0.61 ± 0.13	—	0.28 ± 0.10	—	0.15 ± 0.09	0.21 ± 0.07
$\widetilde{\text{OU}}(\sigma_g^m > 0)$	0.2	0.0	0.30 ± 0.06	0.71 ± 0.10	0.40 ± 0.12	—	0.18 ± 0.13	—	0.02 ± 0.05	0.26 ± 0.06
		0.1	0.32 ± 0.06	0.71 ± 0.09	0.38 ± 0.11	—	0.21 ± 0.12	—	0.02 ± 0.05	0.25 ± 0.06
		0.5	0.46 ± 0.10	0.74 ± 0.10	0.34 ± 0.14	—	0.36 ± 0.10	—	0.03 ± 0.05	0.21 ± 0.07
		1.0	0.56 ± 0.12	0.75 ± 0.10	0.27 ± 0.15	—	0.39 ± 0.09	—	0.04 ± 0.06	0.18 ± 0.08
	0.5	0.0	0.30 ± 0.06	0.68 ± 0.09	0.51 ± 0.10	—	0.14 ± 0.12	0.52 ± 0.06	0.01 ± 0.03	0.26 ± 0.05
		0.1	0.31 ± 0.06	0.68 ± 0.09	0.51 ± 0.12	—	0.15 ± 0.12	—	0.01 ± 0.03	0.25 ± 0.05
		0.5	0.42 ± 0.09	0.67 ± 0.09	0.50 ± 0.13	—	0.30 ± 0.11	0.59 ± 0.04	0.01 ± 0.02	0.24 ± 0.07
		1.0	0.49 ± 0.10	0.66 ± 0.09	0.48 ± 0.16	—	0.32 ± 0.10	0.54 ± 0.06	0.02 ± 0.04	0.22 ± 0.06
	1.0	0.0	0.30 ± 0.05	0.59 ± 0.09	0.56 ± 0.09	—	0.11 ± 0.10	—	0.00 ± 0.02	0.26 ± 0.05
		0.1	0.31 ± 0.06	0.58 ± 0.08	0.58 ± 0.10	—	0.12 ± 0.11	—	0.00 ± 0.01	0.25 ± 0.05
		0.5	0.38 ± 0.08	0.59 ± 0.08	0.61 ± 0.12	—	0.21 ± 0.12	—	0.00 ± 0.02	0.23 ± 0.06
		1.0	0.43 ± 0.08	0.58 ± 0.09	0.62 ± 0.11	—	0.24 ± 0.10	—	0.01 ± 0.03	0.23 ± 0.07

Table 7: F1 Score - $N = 10$, $\sigma_g^a = 0.5$

Dataset	C	σ_b	Granger	PLACy	PCMCI	CCM-Filtering	RCV-VarLiNGAM	Rhino	DYNOTEARS	PCMCI $_{\Omega}$
$\text{OU}(\sigma_g^m = 0)$	0.2	0.0	0.87 ± 0.07	0.17 ± 0.12	0.05 ± 0.09	—	0.46 ± 0.08	—	0.02 ± 0.05	0.07 ± 0.07
		0.1	0.46 ± 0.09	0.22 ± 0.13	0.09 ± 0.10	—	0.45 ± 0.08	—	0.12 ± 0.09	0.08 ± 0.06
		0.5	0.41 ± 0.07	0.16 ± 0.11	0.24 ± 0.10	—	0.40 ± 0.09	—	0.23 ± 0.08	0.10 ± 0.07
		1.0	0.51 ± 0.09	0.13 ± 0.10	0.11 ± 0.10	—	0.41 ± 0.09	—	0.21 ± 0.09	0.12 ± 0.06
	0.5	0.0	0.67 ± 0.08	0.80 ± 0.07	0.16 ± 0.11	—	0.43 ± 0.08	—	0.01 ± 0.02	0.10 ± 0.06
		0.1	0.41 ± 0.07	0.76 ± 0.07	0.12 ± 0.11	—	0.41 ± 0.09	—	0.04 ± 0.07	0.10 ± 0.06
		0.5	0.36 ± 0.06	0.63 ± 0.10	0.29 ± 0.13	—	0.36 ± 0.09	—	0.07 ± 0.10	0.14 ± 0.06
		1.0	0.41 ± 0.06	0.44 ± 0.12	0.19 ± 0.12	—	0.36 ± 0.11	—	0.08 ± 0.10	0.20 ± 0.06
	1.0	0.0	0.59 ± 0.09	0.59 ± 0.09	0.38 ± 0.18	—	0.38 ± 0.08	—	0.00 ± 0.02	0.12 ± 0.06
		0.1	0.40 ± 0.08	0.59 ± 0.09	0.21 ± 0.14	—	0.38 ± 0.08	—	0.04 ± 0.07	0.12 ± 0.06
		0.5	0.33 ± 0.06	0.58 ± 0.09	0.32 ± 0.14	—	0.31 ± 0.10	—	0.12 ± 0.11	0.19 ± 0.07
		1.0	0.36 ± 0.06	0.53 ± 0.09	0.23 ± 0.14	—	0.28 ± 0.10	—	0.13 ± 0.12	0.24 ± 0.07
$\widetilde{\text{OU}}(\sigma_g^m = 0)$	0.2	0.0	0.87 ± 0.07	0.26 ± 0.12	0.06 ± 0.09	—	0.46 ± 0.09	—	0.00 ± 0.00	0.07 ± 0.06
		0.1	0.34 ± 0.06	0.35 ± 0.10	0.12 ± 0.11	—	0.46 ± 0.08	—	0.00 ± 0.00	0.07 ± 0.06
		0.5	0.28 ± 0.05	0.20 ± 0.11	0.25 ± 0.14	—	0.41 ± 0.10	—	0.01 ± 0.04	0.11 ± 0.07
		1.0	0.37 ± 0.05	0.19 ± 0.11	0.15 ± 0.11	—	0.40 ± 0.09	—	0.04 ± 0.06	0.12 ± 0.06
	0.5	0.0	0.67 ± 0.07	0.73 ± 0.07	0.17 ± 0.13	—	0.44 ± 0.08	—	0.00 ± 0.00	0.10 ± 0.06
		0.1	0.33 ± 0.05	0.57 ± 0.07	0.15 ± 0.12	—	0.42 ± 0.09	—	0.00 ± 0.00	0.11 ± 0.06
		0.5	0.28 ± 0.05	0.57 ± 0.09	0.28 ± 0.12	—	0.35 ± 0.10	—	0.00 ± 0.01	0.15 ± 0.07
		1.0	0.34 ± 0.04	0.45 ± 0.10	0.18 ± 0.13	—	0.33 ± 0.09	—	0.02 ± 0.05	0.21 ± 0.07
	1.0	0.0	0.59 ± 0.09	0.54 ± 0.08	0.38 ± 0.19	—	0.37 ± 0.08	—	0.00 ± 0.00	0.13 ± 0.06
		0.1	0.32 ± 0.06	0.47 ± 0.07	0.22 ± 0.13	—	0.36 ± 0.08	—	0.00 ± 0.00	0.13 ± 0.07
		0.5	0.28 ± 0.05	0.53 ± 0.08	0.29 ± 0.14	—	0.32 ± 0.11	—	0.00 ± 0.02	0.18 ± 0.06
		1.0	0.37 ± 0.05	0.48 ± 0.07	0.21 ± 0.12	—	0.30 ± 0.11	—	0.01 ± 0.03	0.24 ± 0.06
$\text{OU}(\sigma_g^m > 0)$	0.2	0.0	0.74 ± 0.09	0.55 ± 0.14	0.13 ± 0.13	—	0.44 ± 0.07	—	0.15 ± 0.09	0.11 ± 0.06
		0.1	0.68 ± 0.10	0.63 ± 0.13	0.15 ± 0.11	—	0.43 ± 0.07	—	0.14 ± 0.08	0.13 ± 0.07
		0.5	0.66 ± 0.09	0.68 ± 0.11	0.14 ± 0.12	—	0.44 ± 0.08	—	0.20 ± 0.07	0.14 ± 0.06
		1.0	0.66 ± 0.09	0.65 ± 0.12	0.11 ± 0.13	—	0.43 ± 0.07	—	0.22 ± 0.07	0.12 ± 0.07
	0.5	0.0	0.60 ± 0.09	0.72 ± 0.09	0.31 ± 0.19	—	0.42 ± 0.07	—	0.03 ± 0.05	0.16 ± 0.07
		0.1	0.57 ± 0.08	0.69 ± 0.09	0.30 ± 0.15	—	0.40 ± 0.08	—	0.02 ± 0.05	0.17 ± 0.07
		0.5	0.56 ± 0.08	0.69 ± 0.08	0.28 ± 0.16	—	0.39 ± 0.09	—	0.08 ± 0.09	0.17 ± 0.07
		1.0	0.57 ± 0.10	0.68 ± 0.08	0.28 ± 0.16	—	0.39 ± 0.10	—	0.08 ± 0.08	0.18 ± 0.07
	1.0	0.0	0.53 ± 0.10	0.58 ± 0.09	0.54 ± 0.17	—	0.34 ± 0.09	—	0.05 ± 0.06	0.18 ± 0.08
		0.1	0.51 ± 0.10	0.58 ± 0.08	0.51 ± 0.16	—	0.35 ± 0.10	—	0.03 ± 0.05	0.18 ± 0.07
		0.5	0.48 ± 0.10	0.58 ± 0.09	0.51 ± 0.16	—	0.32 ± 0.10	—	0.07 ± 0.08	0.21 ± 0.07
		1.0	0.49 ± 0.08	0.58 ± 0.08	0.47 ± 0.16	—	0.31 ± 0.11	—	0.09 ± 0.09	0.21 ± 0.07
$\widetilde{\text{OU}}(\sigma_g^m > 0)$	0.2	0.0	0.28 ± 0.05	0.59 ± 0.14	0.34 ± 0.12	—	0.12 ± 0.13	—	0.03 ± 0.06	0.26 ± 0.05
		0.1	0.28 ± 0.05	0.67 ± 0.12	0.33 ± 0.13	—	0.14 ± 0.13	—	0.02 ± 0.06	0.26 ± 0.05
		0.5	0.42 ± 0.09	0.68 ± 0.11	0.19 ± 0.12	—	0.39 ± 0.09	—	0.03 ± 0.06	0.20 ± 0.07
		1.0	0.60 ± 0.11	0.66 ± 0.10	0.12 ± 0.12	—	0.44 ± 0.08	—	0.05 ± 0.07	0.16 ± 0.07
	0.5	0.0	0.28 ± 0.05	0.70 ± 0.09	0.48 ± 0.13	—	0.10 ± 0.12	—	0.01 ± 0.04	0.27 ± 0.05
		0.1	0.28 ± 0.05	0.69 ± 0.09	0.47 ± 0.13	—	0.14 ± 0.13	—	0.01 ± 0.03	0.27 ± 0.05
		0.5	0.39 ± 0.08	0.70 ± 0.09	0.40 ± 0.16	—	0.34 ± 0.10	—	0.01 ± 0.03	0.22 ± 0.06
		1.0	0.53 ± 0.08	0.69 ± 0.10	0.27 ± 0.17	—	0.38 ± 0.10	—	0.01 ± 0.03	0.18 ± 0.07
	1.0	0.0	0.28 ± 0.05	0.59 ± 0.09	0.56 ± 0.10	—	0.08 ± 0.10	—	0.01 ± 0.03	0.26 ± 0.05
		0.1	0.28 ± 0.05	0.59 ± 0.09	0.56 ± 0.09	—	0.11 ± 0.10	—	0.01 ± 0.03	0.27 ± 0.05
		0.5	0.36 ± 0.07	0.60 ± 0.10	0.54 ± 0.13	—	0.27 ± 0.10	—	0.00 ± 0.02	0.24 ± 0.06
		1.0	0.47 ± 0.08	0.58 ± 0.09	0.47 ± 0.15	—	0.29 ± 0.09	—	0.01 ± 0.02	0.21 ± 0.06

D.3.1 PCMCI in Frequency

We observed that performing causal discovery on the $(\mathbf{a}, \boldsymbol{\lambda})$ parameters leads to significant performance improvements for other CD algorithms. For instance, regarding the **PCMCI** algorithm, Table 8 shows that instead of applying the algorithm directly to the time-domain data, running it on the spectral parameters results in higher F1 scores with a small reduction in TNR in some cases. These results suggest that our preprocessing approach can be beneficial also when applied to other causal discovery paradigms, paving the way for future works in this direction.

Table 8: Performance Improvement - $N = 5$, $\sigma_g^a = 1.0$

	Granger			PCMCI	
	C	F1	TNR	F1	TNR
$\text{OU}(\sigma_g^m = 0)$	0.2	-0.44±0.32	+0.21±0.19	+0.02±0.32	-0.03±0.07
	0.5	+0.16±0.26	+0.21±0.20	+0.38±0.44	-0.03±0.07
	1.0	+0.23±0.26	+0.21±0.21	+0.46±0.34	-0.03±0.08
$\widetilde{\text{OU}}(\sigma_g^m = 0)$	0.2	-0.22±0.35	+0.38±0.30	+0.13±0.39	-0.05±0.10
	0.5	+0.24±0.27	+0.38±0.29	+0.37±0.38	-0.06±0.09
	1.0	+0.25±0.26	+0.34±0.29	+0.42±0.34	-0.05±0.09
$\text{OU}(\sigma_g^m > 0)$	0.2	+0.09±0.28	+0.09±0.10	+0.38±0.37	-0.01±0.05
	0.5	+0.18±0.20	+0.11±0.12	+0.43±0.35	-0.01±0.05
	1.0	+0.20±0.20	+0.13±0.14	+0.27±0.31	0.00±0.05
$\widetilde{\text{OU}}(\sigma_g^m > 0)$	0.2	+0.36±0.25	+0.41±0.24	+0.35±0.35	+0.08±0.10
	0.5	+0.41±0.21	+0.41±0.23	+0.39±0.27	+0.08±0.10
	1.0	+0.39±0.22	+0.40±0.24	+0.31±0.25	+0.08±0.11

D.4 Computational Resources

The experiments were conducted on a high-performance computing cluster comprising 50 DELL EMC PowerEdge R7425 servers, each equipped with dual AMD EPYC 7301 processors (32 cores total per node at 2.2GHz). Among the nodes, 19 are enhanced with NVIDIA Quadro RTX 6000 GPUs (24GB VRAM).

Table 9: Elapsed time for a single experiment (seconds).

N	Granger	PLACy	PCMCI	CCM-Filtering	RCV-VarLiNGAM	DYNOTEARS	PCMCIomega
5	0.16±0.01	5.80±0.01	1.05±0.00	426.35±1.57	1.98±0.10	0.00±0.00	7.06±0.04
10	0.71±0.00	11.94±0.03	4.86±0.03	1924.20±19.32	7.03±0.27	0.00±0.00	44.42±0.13

Regarding **Rhino**, it involves training neural networks, so we used the GPU of our cluster to run it. An experiment of **Rhino** took ~ 4 hours.